Global and Planetary Change xxx (2012) xxx–xxx

Contents lists available at SciVerse ScienceDirect

Global and Planetary Change

journal homepage: www.elsevier.com/locate/gloplacha

Plankton and productivity during the Permian–Triassic boundary crisis: An analysis of organic carbon fluxes

Thomas J. Algeo [a,*], Charles M. Henderson [b], Jinnan Tong [c], Qinglai Feng [c], Hongfu Yin [c], Richard V. Tyson [d]

[a] Department of Geology, University of Cincinnati, Cincinnati, OH 45221, USA
[b] Department of Geoscience, University of Calgary, Calgary, Alberta T2N1N4, Canada
[c] State Key Laboratory of Geological Processes and Mineral Resources, China University of Geosciences, Wuhan 430074, China
[d] GETECH, Kitson House, Elmete Hall, Elmete Lane, Leeds LS8 2LJ, United Kingdom

ARTICLE INFO

Article history:
Received 9 November 2010
Accepted 27 February 2012
Available online xxxx

Keywords:
mass extinction
South China
total organic carbon
sedimentation rates
organic carbon accumulation rates
primary productivity

ABSTRACT

Changes in marine primary productivity following the latest Permian mass extinction (LPME) have been debated at length, with little resolution to date owing to a paucity of quantitative data. Herein, we report total organic carbon (TOC) concentrations and organic carbon accumulation rates (OCAR) for 40 Permian–Triassic boundary (PTB) sections with a near-global distribution and consider their implications for changes in marine productivity during the boundary crisis. Many sections in South China exhibit abrupt declines in TOC and OCAR from the Changhsingian (latest Permian) to the Griesbachian (earliest Triassic), a pattern not observed for sections in other regions. This pattern cannot be explained through secular changes in sedimentation rates, sedimentary facies, or redox conditions, all of which would have favored higher (rather than lower) TOCs and OCARs during the Griesbachian. Further, back-calculation of OC fluxes demonstrate that this pattern cannot be attributed to diagenetic loss of OC in the sediment or, possibly, to OC remineralization in the water column. The most likely explanation is a collapse of marine primary productivity across the South China region concurrently with the LPME and continuing for an extended interval into the Early Triassic. The productivity crash as well as the coeval decimation of benthic marine fauna coincided with deposition of the "boundary clay" at Meishan D, suggesting that both events were related to a large explosive volcanic eruption of uncertain provenance. In other PTB sections having a wide geographic distribution, OCARs increased on average by a factor of ~4× across the LPME, largely owing to a concurrent increase in bulk accumulation rates (BARs). Radiometric dating uncertainties can account at most for only a fraction of the secular change in BARs, which are likely to reflect an increase in subaerial weathering rates and elevated fluxes of detrital material to Early Triassic marine systems. Intensification of chemical weathering relative to physical weathering may have increased the flux of nutrients to the Early Triassic ocean, enhancing marine productivity and contributing to the widespread development of marine dysoxia–anoxia.

1. Introduction

The latest Permian mass extinction (LPME), just prior to the ~252-million-year-old Permian–Triassic boundary (PTB), represents the largest mass extinction in the Phanerozoic record, during which ~90% of marine invertebrate and ~80% of terrestrial vertebrate species disappeared (Erwin et al., 2002; Irmis and Whiteside, 2011). While the ultimate causes of this event remain under discussion (Wignall, 2007), recent work has demonstrated unambiguously that the effects of this event extended to the base of the trophic web in marine ecosystems (Fig. 1). The end-Permian crisis coincided with an abrupt decline in eukaryotic marine phytoplankton (Knoll et al., 2007; Luo et al., this volume), proliferation of prasinophyte and acritarch "disaster taxa" (Payne and van de Schootbrugge, 2007), and a general increase in the abundance of green sulfur and N-fixing cyanobacteria (Grice et al., 2005; Xie et al., 2005, 2007; Hays et al., 2007; Cao et al., 2009; Luo et al., 2011). Cyanobacterial autotrophs may have flourished in the aftermath of the crisis owing to their greater resistance to harsh environmental conditions and a competitive advantage over eukaryotic phytoplankton in anoxic waters rich in ammonium (Knoll et al., 2007). Further, changes in phytoplanktic community (Fig. 1) may have been detrimental to organisms at higher trophic levels in that cyanobacteria generate harmful toxins and do not synthesize the sterols needed by marine invertebrates, as do eukaryotic phytoplankton (Knoll et al., 2007).

Changes in taxonomic diversity and community structure, however, do not necessarily equate with changes in primary productivity rates, which might have been sustained at pre-crisis levels or even have increased following the LPME. At present, no consensus exists concerning changes in nutrient inventories and energy flows in marine ecosystems

* Corresponding author.
E-mail address: Thomas.Algeo@uc.edu (T.J. Algeo).

0921-8181/$ – see front matter © 2012 Elsevier B.V. All rights reserved.
doi:10.1016/j.gloplacha.2012.02.008

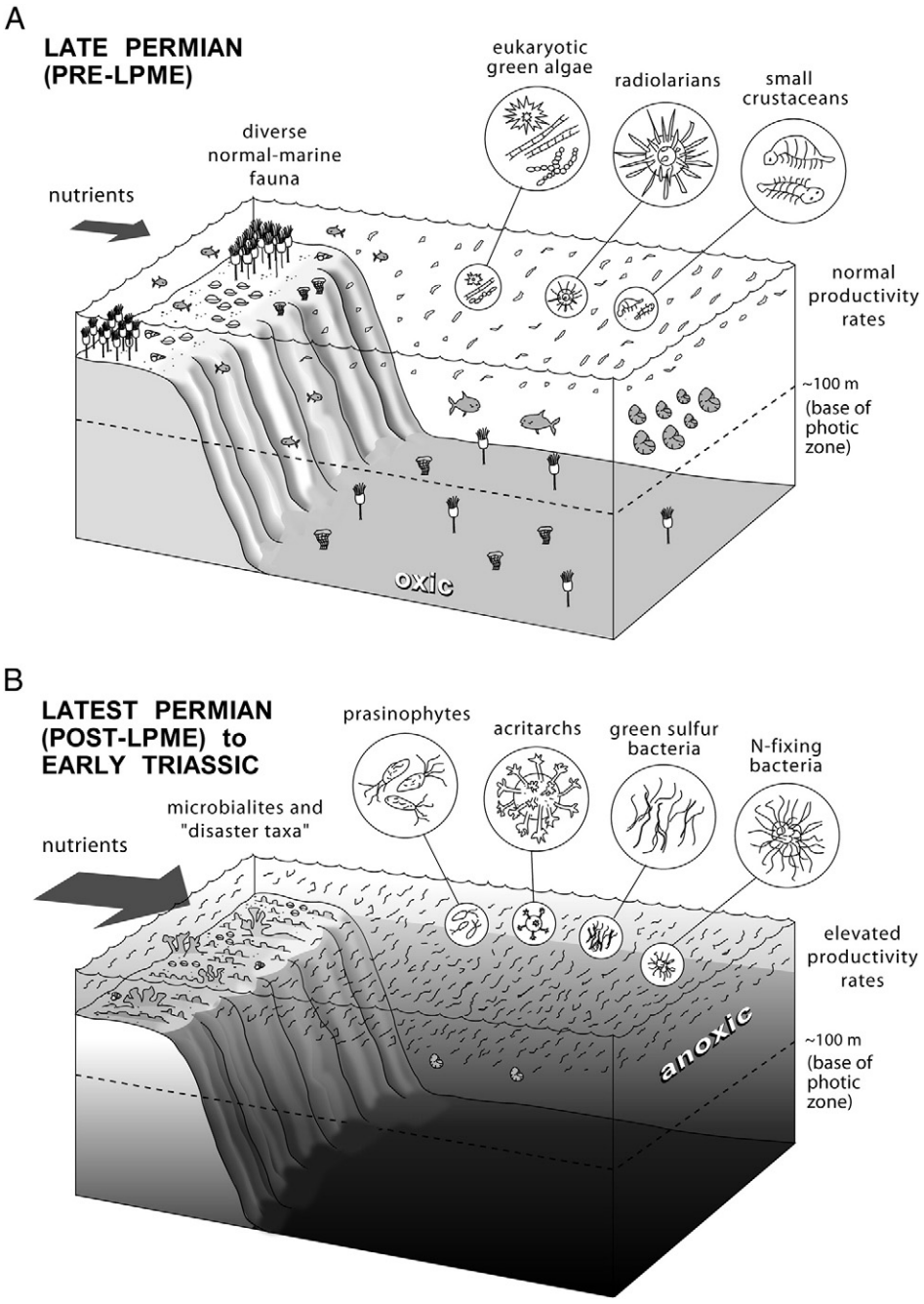

Fig. 1. Interpretative changes in planktic community composition, nutrient fluxes, and primary productivity rates in conjunction with the latest Permian mass extinction (LPME): (A) Changhsingian (i.e., pre-LPME Late Permian only), and (B) Griesbachian (i.e., including the post-LPME latest Permian). Note that this study evaluates changes in OC fluxes across the LPME rather than the PTB.

as a result of the LPME. Martin (1996) claimed that nutrient-poor conditions led to a general collapse of marine primary productivity during the Early Triassic, a view seconded by Rampino and Caldeira (2005) on the basis of the ubiquitous ~3‰ decline in $\delta^{13}C_{carb}$ at the LPME. However, this C-isotopic shift has multiple potential causes (Berner, 2002; Payne and Kump, 2007), and other considerations do not favor Martin's hypothesis. First, global starvation during the Early Triassic is hard to reconcile with the observation that taxa with high rates of basal and exercise metabolism, e.g., many mollusks, disproportionately survived the crisis relative to those with lesser oxygen demands (Rhodes and Thayer, 1991; Knoll et al., 2007). Second, the widespread dysoxia and anoxia in Early Triassic oceans (subsequently "anoxia" for brevity) (Fig. 1; Isozaki, 1997; Meyer et al., 2008; Brennecka et al., 2011) may have been caused in part by higher sinking fluxes of organic matter (Meyer et al., 2011; Winguth and Winguth, 2012). While these considerations argue against strongly diminished rates of marine primary productivity following the LPME, quantitative data bearing on this issue have been lacking to date. The goal of the present study is to assess changes in organic carbon fluxes in conjunction with the LPME, in order to determine the relationship of the end-Permian crisis to changes in marine primary productivity.

Qualitative changes in primary production are commonly inferred in paleoceanographic studies (e.g., Caplan and Bustin, 1999; Cramer and Saltzman, 2005). In contrast, quantitative estimation of primary production in paleomarine systems is inherently difficult owing to large losses of organic carbon (OC) within both the water and sediment columns prior to final preservation. In one early attempt of this type, Bralower and Thierstein (1984) estimated primary production assuming a fixed preservation factor of 2% for organic matter in Cretaceous

Please cite this article as: Algeo, T.J., et al., Plankton and productivity during the Permian–Triassic boundary crisis: An analysis of organic carbon fluxes, Glob. Planet. Change (2012), doi:10.1016/j.gloplacha.2012.02.008

black shales. Most later studies have estimated primary production by applying corrections to measured total organic carbon (TOC) concentrations based on various sediment parameters, e.g., S and Mn concentrations (Vetö et al., 1997), excess Ba fluxes (Thompson, 2000), or amino-acid compositions (Gupta and Kawahata, 2006). Statistical approaches based on microfossil assemblages have been used as well (Lopes et al., 2010). In some cases, the estimates of these studies represent the OC flux to the sediment–water interface rather than primary production in the surface watermass. Similar sequential approaches to the analysis of OC fluxes have been applied to sub-Recent marine sediments (Dunne et al., 2007).

In the present study of marine primary productivity during the LPME crisis, we have undertaken a sequential approach to analysis of OC fluxes. First, we calculated organic carbon accumulation rates (OCAR) for each study section based on measured TOC values and linear sedimentation rates (LSR) determined from an updated Permian–Triassic timescale. Second, we back-calculated OC fluxes at four earlier stages in the depositional history of each study section, prior to (1) late diagenetic OC loss through thermal maturation, (2) early diagenetic OC loss through bacterial sulfate reduction, (3) early diagenetic OC loss through aerobic decay, and (4) OC remineralization in the water column. The estimate derived at step three represents the "sinking flux" of OC (i.e., the flux arriving at the sediment–water interface, or SWI), and the ratio of OCAR to this flux is termed the "burial efficiency" (BE) (Henrichs and Reeburgh, 1987; Tyson, 2005). The estimate derived at step four represents the primary productivity rate (PPR), and the ratio of OCAR to this flux is termed the "preservation factor" (PF) (Bralower and Thierstein, 1984; Tyson, 2005). As discussed below, the OC sinking flux and BE can be estimated with a fair degree of accuracy, making these parameters useful in the analysis of paleomarine systems, but estimates of PPR and PF have large uncertainties and should be regarded as potentially exemplary rather than accurate.

We analyzed OC fluxes for 40 marine PTB sections having a near-global distribution. For each section, we calculated separate fluxes for the Late Permian Changhsingian Stage and the Early Triassic Griesbachian substage (n.b., the latter includes post-LPME beds of latest Permian age because we are evaluating changes in OC fluxes at the LPME rather than the PTB). Although the data presented here do not fully resolve the question of changes in primary productivity rates in conjunction with the LPME, they do provide insights regarding this issue. First, our analysis shows that OCARs and PPRs increased on average globally by a factor of ~4× from the Changhsingian to the Griesbachian. Such a large increase in the organic carbon burial flux implies commensurate increases in the flux of nutrients to the marine photic zone, yet climatic warming following the LPME (Retallack, 1999; Retallack and Jahren, 2008) is likely to have reduced rates of vertical mixing in the global ocean (Hotinski et al., 2001). Instead, increased nutrient availability in shallow-marine environments may have been due to enhanced rates of continental weathering (Fig. 1; Algeo and Twitchett, 2010; Algeo et al., 2011a). Second, our analysis shows that almost all sections from the South China craton record abrupt decreases in OCARs and PPRs in conjunction with the LPME, a pattern not found in any other region globally. We infer that this pattern reflects a collapse of marine primary productivity related to marine environmental changes following the LPME that were specific to the South China region. Such regional patterns may record the spatially variable interplay of changes in nutrient availability, marine primary productivity, and environmental conditions and their attendant consequences for the vitality of contemporaneous marine ecosystems.

2. Methods

2.1. Study sections

The present study makes use of data from 40 independent studies of marine PTB sections (henceforth just "sections"), arranged into four regional groupings: (1) the South China region, with 10 sections; (2) the non-Chinese Tethyan region, with 13 sections; (3) the N&W Pangean region, with 11 sections; and (4) the Panthalassic region, with 6 sections (Fig. 2; Supplement Table 1). The dominant lithologies vary by region, e.g., mainly carbonates in the Tethyan region and mainly siliciclastics in the N&W Pangean and Panthalassic regions (Supplement Table 2), but these lithologic differences are not correlated with variations in bulk accumulation rates (Algeo and Twitchett, 2010, their Fig. 2). Data were drawn from published sources for 24 sections and are original to this study for 16 sections. A few sections (specifically Meishan, China and Bulla, Italy) have been investigated multiple times, with each study treated as an independent record.

2.2. Permian–Triassic timescale

Calculation of OCARs for paleomarine systems (Section 2.3) requires good radiometric age control. The Permian–Triassic timescale has undergone major revisions in recent years (Fig. 3) based on ID-TIMS dating of zircons in volcanic ash layers, mainly from South China (Bowring et al., 1998; Mundil et al., 2004; Ovtcharova et al., 2006), narrowing the age of the PTB to 252.3 ± 0.1 Ma (Mundil et al., 2010) or 252.17 ± 0.06 Ma (Shen et al., 2010, 2011). These studies provide age constraints for key stratigraphic horizons of the present study: (1) 254.14 ± 0.07 Ma for the Wuchiapingian–Changhsingian boundary, (2) 252.28 ± 0.08 Ma for the LPME (Shen et al., 2010, 2011), and (3) 251.2 or 251.3 ± 0.1 Ma for the Induan–Olenekian boundary (Galfetti et al., 2007; Mundil et al., 2010). The substages of the Early Triassic Induan Stage have not been radiometrically dated, but the durations of the Griesbachian and Dienerian have been estimated at 0.731 Myr and 0.270 Myr, respectively, based on spectral analysis of a magnetic susceptibility profile from the West Pingdingshan section near Chaohu, China (Guo et al., 2008). Based on these results, we adopted estimated durations of 1.9 ± 0.1 Myr for the Changhsingian Stage and 0.7 ± 0.1 Myr for the Griesbachian substage (Fig. 3). Note that these durations supersede the estimates of 3.4 ± 1.2 Myr and 0.7 ± 0.4 Myr used by Algeo and Twitchett (2010) in their study of changes in sediment mass fluxes at the PTB.

For sections that have not been dated radiometrically, biostratigraphic correlations provide essential age constraints. In the present study, we have used updated biostratigraphic zonation schemes for hindeodid and gondolellid conodonts (Fig. 3). The Wuchiapingian–Changhsingian boundary in the Tethyan region is defined at Meishan, China by the first appearance datum (FAD) of *Clarkina wangi* within a chronomorphocline from *C. longicuspidata* to *C. wangi* (Jin et al., 2006). The FAD of *Hindeodus parvus* at Meishan defines the PTB (Yin et al., 2001). The boundary between the Griesbachian and Dienerian substages of the Early Triassic Induan Stage corresponds to the contact between the *Neoclarkina discreta* and *Sweetospathodus kummeli* zones (the latter referred to the genus *Neospathodus* by Chinese workers, e.g., Zhao et al., 2007; Guo et al., 2008). A taxonomic revision of Late Permian–Early Triassic conodont faunas of the boreal region by C. Henderson is in progress, but existing data (Henderson, 1997; Mei and Henderson, 2001; Henderson and Mei, 2007; Nakrem et al., 2008; Algeo et al., 2012) are sufficient for accurate correlations with Tethyan region faunas. See Supplement Section 1 for a fuller discussion of the biostratigraphic framework used in the present study.

2.3. TOC concentrations and organic petrography

For PTB sections original to this study, sample aliquots were digested in 2 N HCl at 50 °C for 6 h to dissolve carbonate minerals, and the residue was filtered, rinsed, and dried. TOC was measured using an Eltra 2000 C-S analyzer at the University of Cincinnati. Data quality was monitored via multiple analyses of USGS SDO-1 as well as internal lab standards, yielding analytical precisions (2σ) of ± 2.5% of reported values. Mean

Please cite this article as: Algeo, T.J., et al., Plankton and productivity during the Permian–Triassic boundary crisis: An analysis of organic carbon fluxes, Glob. Planet. Change (2012), doi:10.1016/j.gloplacha.2012.02.008

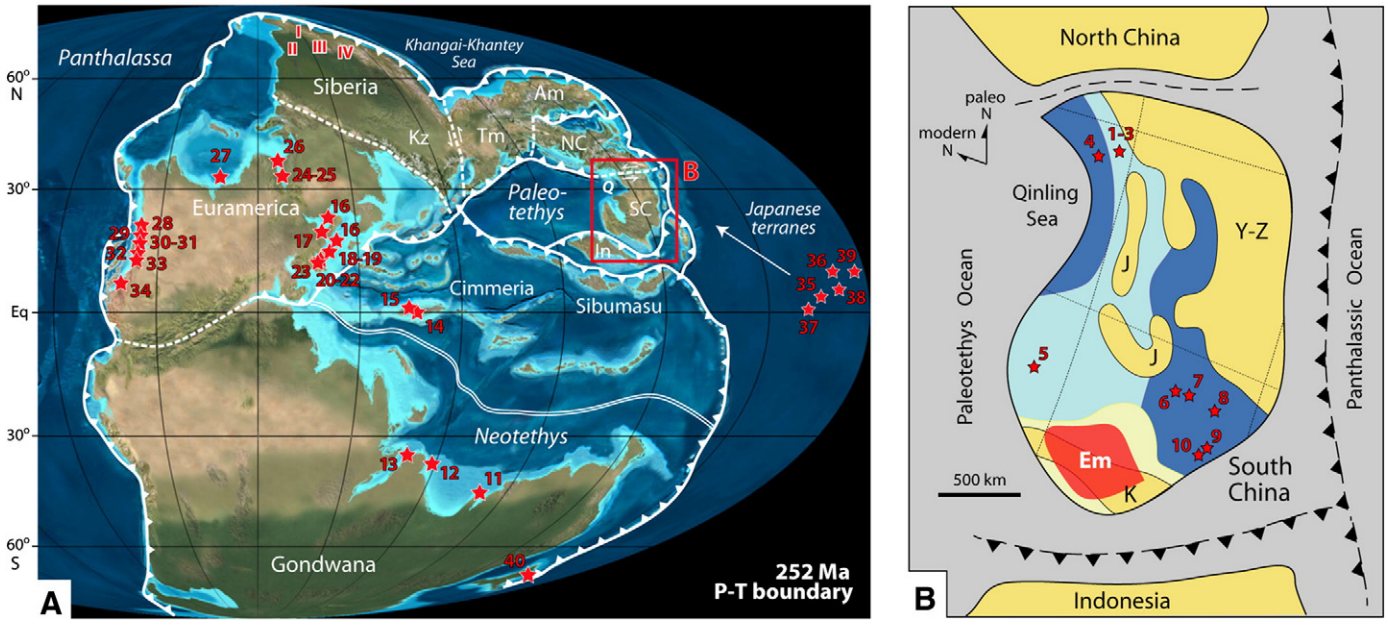

Fig. 2. Paleogeography of (A) the world and (B) South China at the PTB (~252 Ma). Numbering of study sites conforms to Supplement Table 1 and Fig. 6. Abbreviations in A: I–IV = Siberian Traps volcanic centers (in order, Maymecha-Kotuy, Noril'sk, Putorana, and Nizhnyaya Tunguska; Czamanske et al., 1998), Am = Amuria, In = Indonesia, Kz = Kazakhstan, NC = North China, Q = Qinling Ocean, SC = South China, Tm = Tarim. Abbreviations in B: Em = Emeishan flood basalts, J = Jiangnan Uplift, K = Khamdian Uplift, N = Nanpanjiang Basin, Y–Z = Yunkai–Zhemin Uplifts. Note: 70° counterclockwise of South China craton relative to its modern orientation (Nie, 1991).
Base map courtesy of Ron Blakey (http://jan.ucc.nau.edu/~rcb7/); plate boundaries adapted from Scotese and Langford (1995) and Stampfli and Borel (2001); approximate locations of Japanese terranes from Mizutani (1987) and Ando et al. (2001); and facies patterns from Bao (1998).

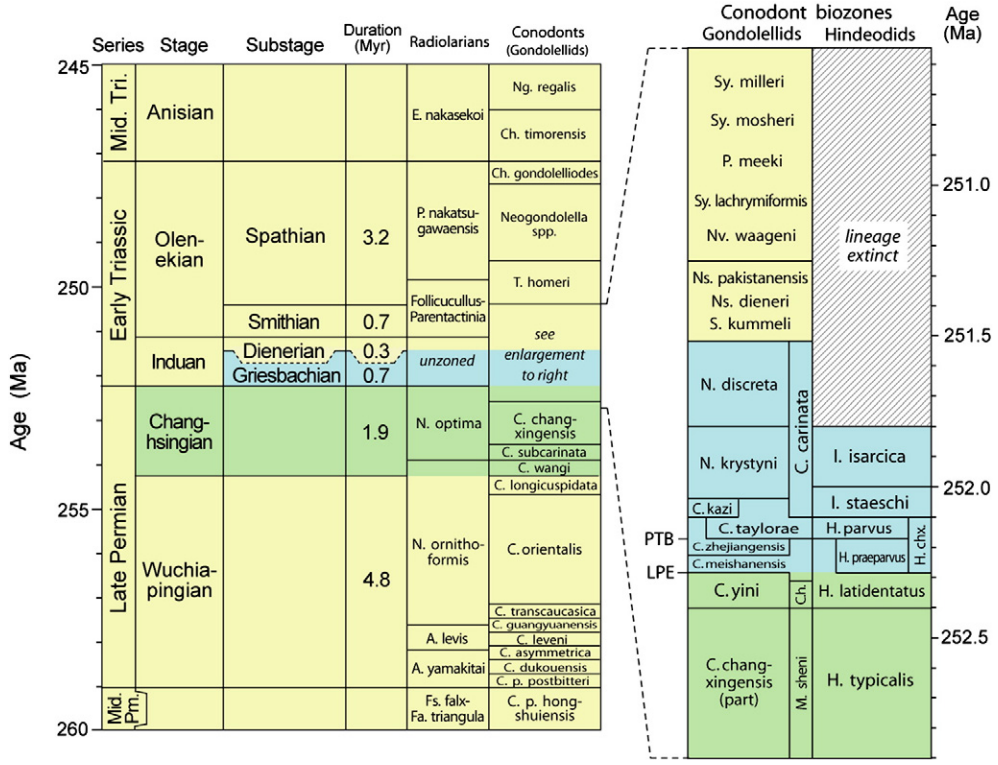

Fig. 3. Late Permian–Early Triassic timescale and biostratigraphic zonation. The present study adopts durations for the Changhsingian (green field) and Griesbachian (blue field) of 1.9 ± 0.1 Myr and 0.7 ± 0.1 Myr, respectively. Radiolarian genera: A. = *Albaillella*, E. = *Eptingium*, Fa. = *Foremanhelena*, Fs. = *Follicucullus*, N. = *Neoalbaillella*, P. = *Parentactinia* (from Sugiyama, 1997; Kuwahara et al., 1998; Xia et al., 2005). Conodont genera: C. = *Clarkina*, Ch. = *Chiosella*, H. = *Hindeodus*, I. = *Isarcicella*, M. = *Mesogondolella*, N. = *Neoclarkina*, Ng. = *Neogondolella*, Nv. = *Novispathodus*, P. = *Paulella*, S. = *Sweetospathodus*, Sy. = *Scythogondolella*, T. = *Triassospathodus*; note that *p. postbitteri* and *p. hongshuiensis* are subspecies of *Clarkina postbitteri*. The enlargement at right shows biozones around the Permian–Triassic boundary (PTB) and latest Permian event (LPME); C. h. = *C. hauschkei*, H. chx. = *H. changxingensis*. Conodont biozonation was updated for the present study by C. M. Henderson. (For interpretation of the references to color in this figure legend, the reader is referred to the web version of this article.)

Please cite this article as: Algeo, T.J., et al., Plankton and productivity during the Permian–Triassic boundary crisis: An analysis of organic carbon fluxes, Glob. Planet. Change (2012), doi:10.1016/j.gloplacha.2012.02.008

TOC values were based on all measurements for the Changhsingian and Griesbachian in a given study section.

For sections original to this study, a subset of samples was examined petrographically to evaluate organic matter sources. In all sections, the majority of samples contained primarily (>90%) amorphous organic matter derived from marine phytoplankton or bacteria. Only a few samples, located mostly at or just above the LPME, contained high concentrations (>50%) of terrestrial organic matter. Published studies for some PTB sections provided additional petrographic or organic geochemical documentation of organic carbon sources—see Supplement Section 2.1 for further discussion.

2.4. Sedimentation rate and burial flux calculations

TOC concentration generally is not a good proxy for OC fluxes because of variable dilution by non-organic components of the sediment:

$$TOC(\%) = f_{OC}/(f_{OC} + f_{DIL}) \times 100\% \quad (1)$$

where f_{OC} is the burial flux of OC (n.b., the non-carbon fraction of organic matter has been disregarded) and f_{DIL} is the diluent flux of non-organic materials to the sediment (cf. Tyson, 2001). Use of OCARs (=OC burial flux, or f_{OC}) allows assessment of the production and preservation of organic matter independently of the flux of non-organic materials (Fig. 4A). Calculation of OCARs in paleomarine systems requires knowledge of sedimentation rates for the stratigraphic interval of interest. For each study site, we calculated a linear sedimentation rate (LSR) for each of the two time-stratigraphic units of interest (i.e., the Changhsingian and Griesbachian) as the full thickness of the time-stratigraphic unit divided by its duration (see Section 2.2). For a few sections, LSRs were determined from age models based on time-series analysis (e.g., Algeo et al., 2010, 2011b). Bulk accumulation rates (BAR) and organic carbon accumulation rates (OCAR) were calculated as:

$$BAR = LSR \times \rho \quad (2)$$

$$OCAR = TOC \times LSR \times \rho \quad (3)$$

where both BAR and OCAR have units of g m^{-2} yr^{-1}, LSR has units of m Myr^{-1}, and ρ is sediment bulk density in units of g cm^{-3} (Fig. 4A). Bulk densities were not available for most study units and, for convenience, were assumed to be 2.5 g cm^{-3} for all samples. None of the study samples exhibited any visible porosity, although shales commonly contain ~3–20% microporosity that is not evident petrographically but results in slightly lower densities than for other lithologies (Rowan et al., 2003). However, suites of cogenetic samples rarely exhibit >10% variation in bulk density (e.g., Schmoker, 1977), and this level of uncertainty is too small to have much influence on the patterns of variation in BARs and OCARs documented in the present study.

2.5. Pre-burial organic carbon flux estimates

OCAR is a measure of the burial flux of OC based on the preserved quantity of TOC in marine sediments (Fig. 4A). However, only a small fraction of primary production survives remineralization in the water column and destruction through diagenetic processes in the sediment. The degree of OC loss varies among the study sections as a function of differences in burial temperatures, organic matter types, redox conditions, porewater chemistry, water depths, and other factors. We estimated the stepwise loss of OC in each study section by using a series of transfer functions based on quantitative studies of OC fluxes in modern marine systems (Fig. 5). Beginning with the burial flux of organic carbon (OCAR, or f_{OC}), we sequentially back-calculated OC fluxes at four earlier stages in the depositional/diagenetic history of each section, prior to (1) late diagenetic OC loss through thermal maturation, (2) early diagenetic OC loss through bacterial sulfate reduction, (3) early diagenetic OC loss through aerobic decay, and (4) OC remineralization in the water column (Fig. 4B). These reconstructed fluxes are designated f_{OC}', f_{OC}'', f_{OC}''' (=OC sinking flux), and f_{OC}'''' (=PPR), respectively. This is a useful approach because it allows estimation of OC fluxes at several stages prior to final burial as well as the compounding of uncertainties associated with successive calculation steps in order to reflect the more tenuous nature of flux estimates at earlier stages. As discussed below, estimates of f_{OC}''' and BE are probably reliable with an uncertainty of a factor of ~2.5×, but estimates of f_{OC}'''' and PF are likely to have substantially higher levels of uncertainty. Thus, the results of this approach are necessarily tentative and should be viewed only as a rough guide to large-scale changes in OC fluxes during the Permian–Triassic transition.

In the first step of the back-calculation process, we estimated f_{OC}' based on a transfer function developed from Raiswell and Berner's (1987) study of OC loss due to thermal maturation of sediments (Fig. 5A). Relative to the average C_{org}/S ratio (2.8) of modern marine muds, they noted that ancient shales exhibit progressively lower C_{org}/S ratios with increasing thermal maturation. OC loss is ca. 40–50% for shales having vitrinite reflectance (R_o) values of 0.8 to 1.0% (corresponding to the peak of the "oil window," or 80–100 °C; Hunt,

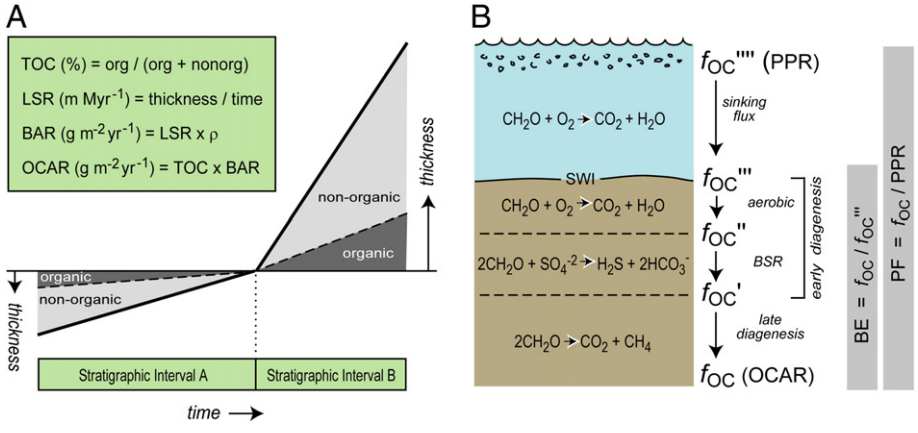

Fig. 4. (A) Model of relationships among total organic carbon (TOC), linear sedimentation rate (LSR), bulk accumulation rate (BAR), and organic carbon accumulation rate (OCAR). OCAR is a function of both TOC, the ratio of organic carbon to total sediment mass, and BAR, a measurement of bulk sediment flux based on time–thickness relationships and average sediment density (ρ); see Eqs. (2) and (3). (B) Model of back-calculated pre-burial OC fluxes in paleomarine systems. f_{OC} (=OCAR) is based on preserved TOC in the sediment, f_{OC}' is the OC flux prior to late diagenetic thermal loss, f_{OC}'' is the OC flux prior to early diagenetic bacterial sulfate reduction (BSR), f_{OC}''' is the OC flux prior to early diagenetic aerobic decay (=OC sinking flux), and f_{OC}'''' is the primary productivity rate (PPR). The burial efficiency (BE) is given by f_{OC}/f_{OC}''', the ratio of preserved OC to the sinking flux, and the preservation factor (PF) by f_{OC}/PPR, the ratio of preserved OC to primary production. SWI=sediment–water interface.

Please cite this article as: Algeo, T.J., et al., Plankton and productivity during the Permian–Triassic boundary crisis: An analysis of organic carbon fluxes, Glob. Planet. Change (2012), doi:10.1016/j.gloplacha.2012.02.008

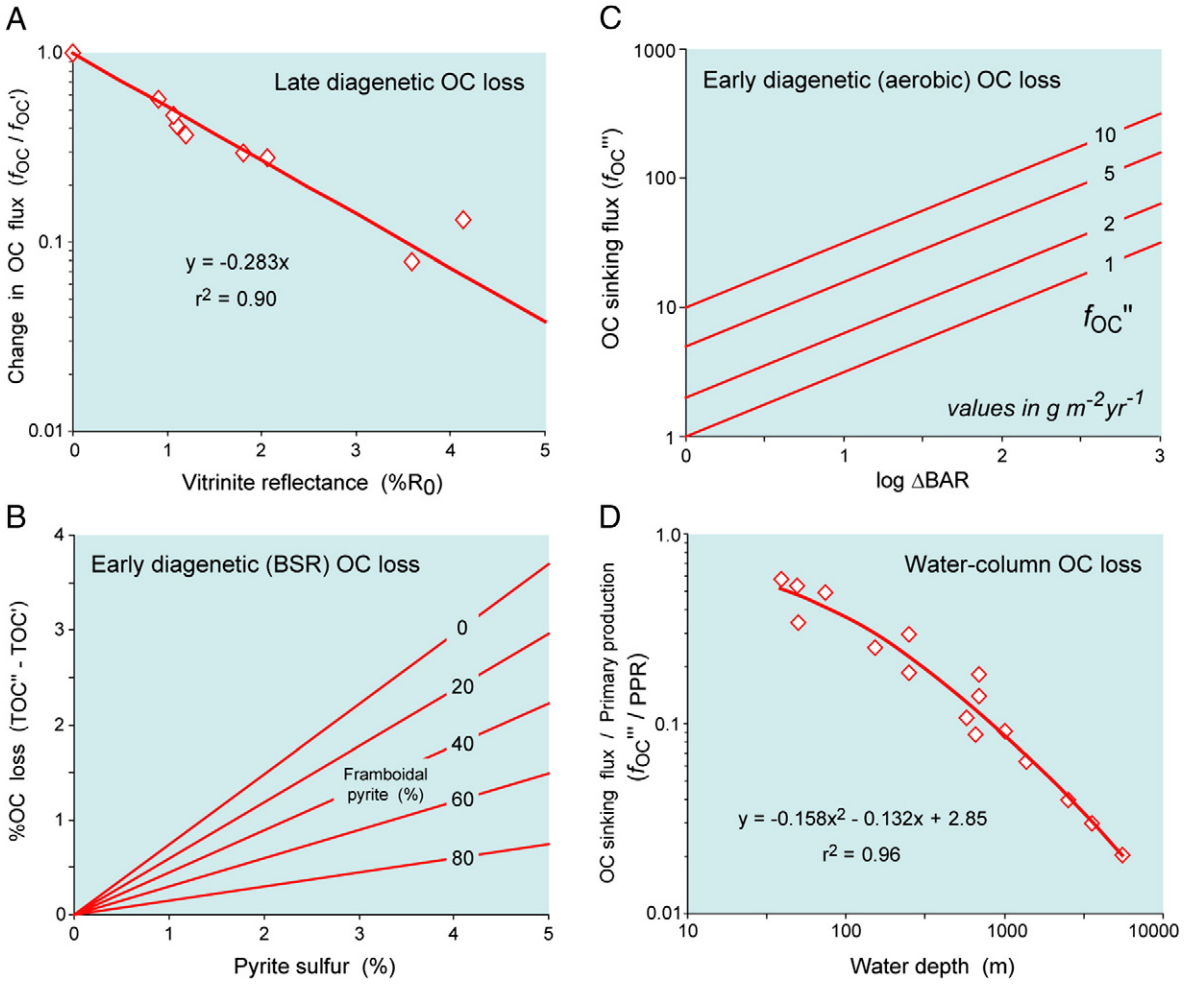

Fig. 5. Transfer functions for back-calculation of pre-burial OC fluxes in paleomarine systems: (A) f_{OC}' (Eq. (4)), (B) f_{OC}'' (Eqs. (5)–(7)), (C) f_{OC}''' (Eq. (8); =OC sinking flux), and (D) f_{OC}'''' (Eq. (9); =PPR). Note that thermal maturity (as proxied by $\%R_o$; Eq. (4)) and water depth (Eq. (9)) are general parameters for a given section that have equal effects on calculated OC fluxes for the Changhsingian and Griesbachian and, hence, result in no secular differential for a section of interest. In contrast, early diagenetic OC losses due to BSR (as proxied by non-framboidal reduced S concentrations; Eq. (6)) and aerobic decay (as proxied by BAR; Eq. (8)) varied secularly at each depositional site, yielding differences in the calculated OC fluxes for the Changhsingian and Griesbachian of a given study section (cf. Fig. 9C).
Panel A is based on Raiswell and Berner (1987), B on Berner (1984), C on Canfield (1994), and D on Meyers (1997); see text for discussion.

1996, p. 368), climbing to 80–90% for shales having R_o of 2.5 to 3.5% (equivalent to low-grade metamorphism, or ~200–250 °C). If the initial C_{org}/S ratio of 2.8 is set to zero, Raiswell and Berner's relationship can be reformulated as:

$$\log(f_{OC}/f_{OC}') = -0.283R_o \quad (4)$$

where f_{OC}/f_{OC}' is the change in organic carbon flux as a result of themal loss of OC during late diagenesis. This relationship accounts for 90% of variance (r^2) in Raiswell and Berner's dataset. See Supplement Section 2.2 for documentation of $\%R_o$ and maximum burial temperatures for the study sections.

In the second step of the back-calculation process, the minimum amount of OC lost through bacterial sulfate reduction (BSR) can be estimated from authigenic pyrite concentrations (Fig. 5B; Berner, 1984; Zaback et al., 1993), assuming that the H_2S produced through this reaction has not migrated vertically any substantial distance within the sediment. The stoichiometry of the reaction is given by:

$$2CH_2O + SO_4^{-2} \rightarrow H_2S + 2HCO_3^- \quad (5)$$

where the composition of sedimentary organic matter is that of a simple sugar (e.g., sucrose, $C_6H_{12}O_6$). Thus, each mole of sulfate S can oxidize 2 mol of organic carbon. The H_2S produced via this reaction is partially trapped in the sediment through (1) sulfidization of organic matter (Vetö et al., 1997; Tribovillard et al., 2004), and (2) reaction with ferrous iron to form first Fe-monosulfides such as mackinawite and greigite and later Fe-disulfides such as pyrite (Berner, 1970; Benning et al., 2000). However, syngenetic framboidal pyrite (i.e., pyrite formed in the water column owing to the presence of dissolved H_2S) does not represent decay of organic matter within the sediment, and this fraction must be subtracted in order to correctly calculate H_2S production due to BSR within the sediment. We estimate the (minimum) OC loss (TOC″ − TOC′) due to early diagenetic BSR as:

$$TOC''–TOC' = 0.75 \times S_{pyrite} \times (1–F_{fram}) \quad (6)$$

where the coefficient 0.75 is the weight ratio representing consumption of 2 mol of reduced carbon (C = 12.01 amu) for each mole of H_2S produced (S = 32.065 amu), and F_{fram} represents the fraction of pyrite sulfur present as syngenetic framboids. See Supplement Section 2.3 for discussion of pyrite S concentrations in the study sections. The OC flux at the aerobic/anaerobic (O_2/H_2S) boundary in the sediment is thus:

$$f_{OC}'' = f_{OC}' + (TOC''–TOC') \times BAR \quad (7)$$

We cannot determine uncertainties for TOC″ − TOC′ estimates of the present study, but where C and S fluxes have been measured in modern

marine systems, the relationship between OC loss due to BSR and sediment reduced S concentrations typically yields r^2 values > 0.90 (e.g., Martens and Klump, 1984; Bertrand and Lallier-Vergès, 1993).

Other approaches to estimating OC loss due to BSR are possible. Berner (1978) used sulfate concentration gradients immediately below the SWI to argue that the amount of organic carbon oxidized by BSR (G_0 in his terminology) is relatively constant in most marine systems (~250–350 mM, or ~0.2–0.8 wt.% of the sediment), provided that BSR is sulfate-limited rather than OC-limited. This estimate assumes an initial porewater sulfate concentration equal to that of modern seawater (~28 mM; Wright and Colling, 1995), but seawater sulfate concentrations are likely to have been considerably lower during the Permian–Triassic transition. Studies of brine inclusions in halite yielded an estimate of ~20 mM for the Late Permian (Horita et al., 2002; Lowenstein et al., 2005), and modeling of CAS $\delta^{34}S$ variation yielded an even lower estimate (~4 mM) for the Early Triassic (Luo et al., 2010). If initial sediment porewater sulfate concentrations were lower by 30–90%, then proportionately less OC would have been oxidized by BSR, with upper limits of ~0.6% and ~0.1% by weight during the Late Permian and Early Triassic, respectively. In the present study sections, the median reduced S concentration is 0.10% for both Upper Permian and Lower Triassic units, equivalent to 0.075% of oxidized OC (per Eq. (6)), a value that is consistent with low concentrations of dissolved sulfate in seawater of that age.

In the third step of the back-calculation process, the amount of OC lost via aerobic decay in the upper part of the sediment column (i.e., above the O_2/H_2S boundary) was estimated based on differences in OC preservation rates between oxic and anoxic facies as a function of BAR (Fig. 5C; Canfield, 1994; Tyson, 2001, 2005). At low BARs, oxic facies undergo strong OC loss via aerobic decay prior to entering the zone of BSR, but anoxic facies exhibit far less OC loss (i.e., higher OCARs for a given BAR) owing to a lack of aerobic decay (see Section 3.4). At high BARs, sediments in all facies are buried quickly and the minimal time in transit from the SWI to the zone of BSR results in little or no aerobic decay, yielding similar OCARs in oxic and anoxic facies at a given BAR. The difference in OCARS between oxic and anoxic facies at a given BAR reflects the average amount of OC loss due to aerobic decay, a relationship that can be quantified as:

$$f_{OC}''' = f_{OC}'' \times \exp_{10}(0.51 \times \Delta BAR) \quad (8)$$

where ΔBAR is the difference in log units (g m^{-2} yr^{-1}) between 3.1 and the BAR of the section of interest (n.b., 3.1 being the BAR at which the oxic and anoxic OCAR trends converge and, hence, above which no aerobic loss of OC occurs; see Section 3.4), and the coefficient 0.51 is the difference in slopes of the OCAR trends of the oxic and anoxic facies (i.e., $\partial(f_{OC}'''-f_{OC}'')/\partial$BAR, or the rate of aerobic loss of OC as a function of BAR). The slopes of the OCAR trends for oxic and anoxic facies have uncertainties of ±0.08 and ±0.25 (log units), respectively, yielding a cumulative uncertainty of ±0.33 for the coefficient 0.51, equivalent to an uncertainty factor of ~2× in calculated values of f_{OC}'''.

The foregoing relationships allow determination of the burial efficiency (BE), i.e., the fraction of OC deposited at the SWI that is ultimately preserved in the sediment (Henrichs and Reeburgh, 1987; Tyson, 2005), as f_{OC}/f_{OC}''' (Fig. 4B). Other algorithms have been used for BE, for example, in their forward calculation of OC fluxes based on modern marine productivity data, Dunne et al. (2007) estimated BE as a function of the sinking flux of OC (their Eq. (3)), a procedure that was claimed to account for ~66% of the variance in OC burial fluxes. However, our procedure has the advantage of basing BE estimates on quantifiable petrographic and geochemical properties of the sediment.

In the fourth step of the back-calculation process, we estimated the amount of OC lost to remineralization during transit through the oceanic water column (Fig. 5D). Modern marine primary productivity exhibits only a weak relationship to both the export flux from the photic zone (Dunne et al., 2005) and the bottom flux (Dunne et al., 2007;="sinking flux" of this study), so estimates of PPR for paleomarine systems are perforce highly uncertain. However, we have estimated PPRs for the study sections for the sake of full development of our procedure for back-calculation of OC fluxes in paleomarine systems. Although numerous factors influence OC loss between the photic zone and the seafloor, including organic matter lability, ballasting, and water-column redox conditions, the single variable that accounts for the largest amount of variance is water depth, which scales positively with residence time of organic matter in the water column and, hence, exposure to aerobic decay (Hedges et al., 1988; Meyers, 1997; Dunne et al., 2007). Further, as a proxy for OC loss in the water column, water depth has the advantage of being readily quantifiable through facies analysis of paleomarine systems. We quantify changes in organic carbon flux during sinking as:

$$f_{OC}'''/f_{OC}'''' = -0.158d^2 - 0.132d + 2.85 \quad (9)$$

where d is water depth in meters. This 2nd-order polynomial equation represents a best fit to the relationship shown in Fig. 2 of Meyers (1997) and accounts for 96% of variance (r^2) in his dataset. Note that f_{OC}'''' is equivalent to primary productivity rate (PPR), and that f_{OC}/f_{OC}'''' is equivalent to the preservation factor (PF), i.e., the fraction of primary production ultimately preserved in the sediment (Bralower and Thierstein, 1984; Tyson, 2005). It should be emphasized that, because the ratio f_{OC}/f_{OC}'''' is typically quite small (averaging ~0.01), all estimates of PPR based on the burial flux of OC (f_{OC}) are highly tentative. Calculated values of PPR for the study sections should be viewed only as indicative of broad regional or temporal trends rather than as accurate for individual units. See Supplement Section 2.4 for discussion of the depositional water depths of the study sections.

The uncertainties associated with OC flux estimates become progressively larger at each subsequent step in the back-calculation procedure, because the uncertainty at any given step is the product of the uncertainties of all steps up to that point. As discussed above, the step-specific uncertainties for estimates of f_{OC}', f_{OC}'', f_{OC}''', and f_{OC}'''' are approximately ±10% (i.e., 1/0.90), <±10% (i.e., 1/>0.90), ±2×, and ±4% (i.e., 1/0.96), respectively. The product of these individual uncertainties yields an estimate of the cumulative uncertainty for f_{OC}'''' (PPR), which is equal to a factor of ~2.5× (see Section 3.5). We regard this value as a reasonable estimate of the uncertainty attached to f_{OC}''' and BEs (rather than f_{OC}'''' and PFs), making estimates of these parameters tentative but constrained sufficiently as to permit a meaningful analysis of variation in OC fluxes in paleomarine systems. On the other hand, the true uncertainties attached to estimates of f_{OC}'''' and PFs are almost certainly larger than a factor of 2.5×. That the water depth–OC flux relationship of Meyers (1997; Fig. 5D) is too well-defined, and its attendant uncertainty of ±4% too small, is indicated by the strong regional variability in organic matter fluxes reported in studies of modern marine systems (e.g., Bishop, 1989; Schlüter et al., 2000; Dunne et al., 2005, 2007). Dunne et al. (2005) showed that export ratios (i.e., the fraction of primary productivity exported from the photic zone) can range from 0.04 to 0.72, meaning that PPRs are between 50% (1/0.72) and 2500% (1/0.04) greater than the export flux, a range of variance that effectively makes accurate back-calculation of PPRs and PFs impossible for paleomarine systems.

3. Results

3.1. Total organic carbon

Total organic carbon (TOC) profiles for a representative subset of the 40 study sections are shown in Fig. 6 and relevant parameters are given in Supplement Table 1. Sections from across the South China craton exhibit an abrupt decline in TOC concentrations following the LPME (Fig. 6A). Mean TOCs for the Changhsingian range from

Please cite this article as: Algeo, T.J., et al., Plankton and productivity during the Permian–Triassic boundary crisis: An analysis of organic carbon fluxes, Glob. Planet. Change (2012), doi:10.1016/j.gloplacha.2012.02.008

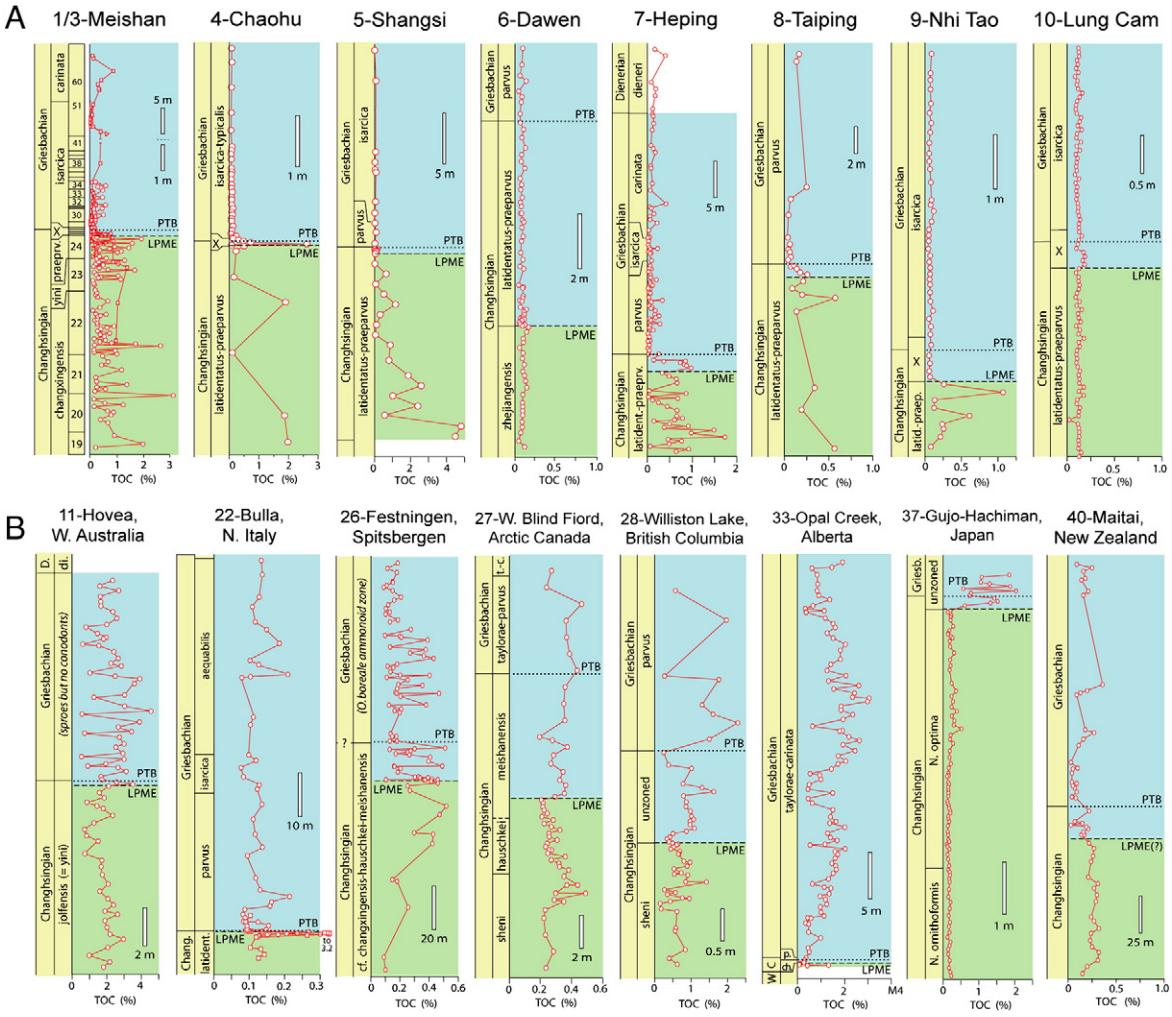

Fig. 6. TOC chemostratigraphy of Permian–Triassic boundary (PTB) sections in (A) South China and (B) elsewhere. Note the pronounced decrease in TOC at the latest Permian mass extinction (LPME) horizon in most South China sections and the absence of a similar decline in most other sections. X = *meishanensis-zhejiangensis-parvus-staeschi* (i.e., closely spaced conodont zones around the PTB); D. = Dienerian, di. = *dieneri*, t.-c. = *taylorae-carinata*. Green and blue fields denote stratigraphic intervals used in OC flux calculations for the Changhsingian and Griesbachian, respectively. Data given in Supplement Table 1. (For interpretation of the references to color in this figure legend, the reader is referred to the web version of this article.)

0.11% at Dawen to 1.31% at Shangsi but decline in the Griesbachian to <0.25% at Meishan and <0.12% in all of the remaining sections. The secular decline in TOC is large in 6 out of 8 sections (reaching a maximum of −97% at Shangsi), although two sections (Dawen and Lung Cam) show little change as a consequence of having low TOCs (<0.20%) in the Changhsingian as well as the Griesbachian. This pattern of declining TOC concentrations across the LPME in South China contrasts strongly with stable or increasing TOC concentrations in most PTB sections elsewhere (Fig. 6B). In the Tethyan region, non-Chinese sections contain up to 2.1% TOC in the Changhsingian and generally exhibit limited relative change across the LPME, as in Slovenia (+10%), at Spiti in northern India (−5%), and in the Hovea-3 drillcore from western Australia (+26%). On the northern and western margins of Euramerica, most sections exhibit comparatively high TOC (~0.5–2.0%) in the Changhsingian and a relative increase across the LPME, as at West Blind Fiord on Ellesmere Island (+19%), in the Peace River Basin of northern Alberta (+2 to +74%), and in southern Alberta and Nevada (>+200%). Exceptions are Schuchert Dal in eastern Greenland and Crooked Creek in southern Alberta, which exhibit relative declines in TOC of −22 to −44% and −52%, respectively. Deep-sea chert sections from the western Panthalassic region exhibit low (<0.25%) TOC in the Changhsingian and relative increases across the LPME ranging from +64% at Taho to >+1000% at Tenjinmaru. However, the predominantly siliciclastic section from Maitai, New Zealand, shows a relative decline of −42%. Thus, PTB sections show TOC chemostratigraphic patterns that are, for the most part, regionally consistent.

3.2. Regional patterns in TOC, LSR and OCAR

The four study regions exhibit broadly dissimilar patterns of mean TOC concentrations for the Changhsingian versus the Griesbachian (Fig. 7A). Sections from South China commonly show higher values in the Changhsingian (0.57 ± 0.13%) than in the Griesbachian (0.12 ± 0.02%; as used here and subsequently, representing the mean plus or minus one standard deviation). In non-Chinese Tethyan sections, the Changhsingian and Griesbachian contain roughly equal amounts of TOC (0.54 ± 0.19% vs. 0.55 ± 0.24%). In N&W Pangean sections, the Griesbachian is somewhat enriched in TOC relative to the Changhsingian (0.84 ± 0.19% vs. 0.58 ± 0.17%), and in Panthalassic sections the Griesbachian is strongly TOC-enriched relative to the Changhsingian (0.65 ± 0.30% vs. 0.10 ± 0.04%). The mean for all study sections shows no statistically significant difference between the Changhsingian (0.49 ± 0.09%) and the Griesbachian (0.54 ± 0.11%). Thus, the regionally averaged data confirm the uniqueness of the abrupt decline in TOC across the LPME for South China sections.

LSRs increase across the LPME in most study sections and in all four regions, although regionally different patterns are evident

(Fig. 7B). For the Changhsingian, mean LSRs vary by nearly an order of magnitude in the following sequence: N&W Pangea (4.7 ± 1.7 m Myr^{-1}), Panthalassa (6.7 ± 1.9 m Myr^{-1}), non-Chinese Tethys (19 ± 8 m Myr^{-1}), and South China (36 ± 7 m Myr^{-1}). For the Griesbachian, mean LSRs vary by more than an order of magnitude in the following sequence: Panthalassa (8.0 ± 5.5 m Myr^{-1}), non-Chinese Tethys (53 ± 20 m Myr^{-1}), South China (102 ± 16 m Myr^{-1}), and N&W Pangea (120 ± 29 m Myr^{-1}). Mean LSRs increase from the Changhsingian to the Griesbachian by a factor of <2× for Panthalassa, ~3× for the non-Chinese Tethys and South China, and ~25× for N&W Pangea. The only sections to show a secular decline in accumulation rates are deep-sea chert successions from Japan, in which LSRs decrease by a factor of 0.95× to 0.10× across the LPME. The mean LSR of all study sections is a factor of ~4.5× greater for the Griesbachian (59 ± 13 m Myr^{-1}) than for the Changhsingian (13 ± 3 m Myr^{-1}). Because BARs are related to LSRs by an invariant parameter (ρ; see Eq. (2)), they show the same patterns of variation in time and space as LSRs.

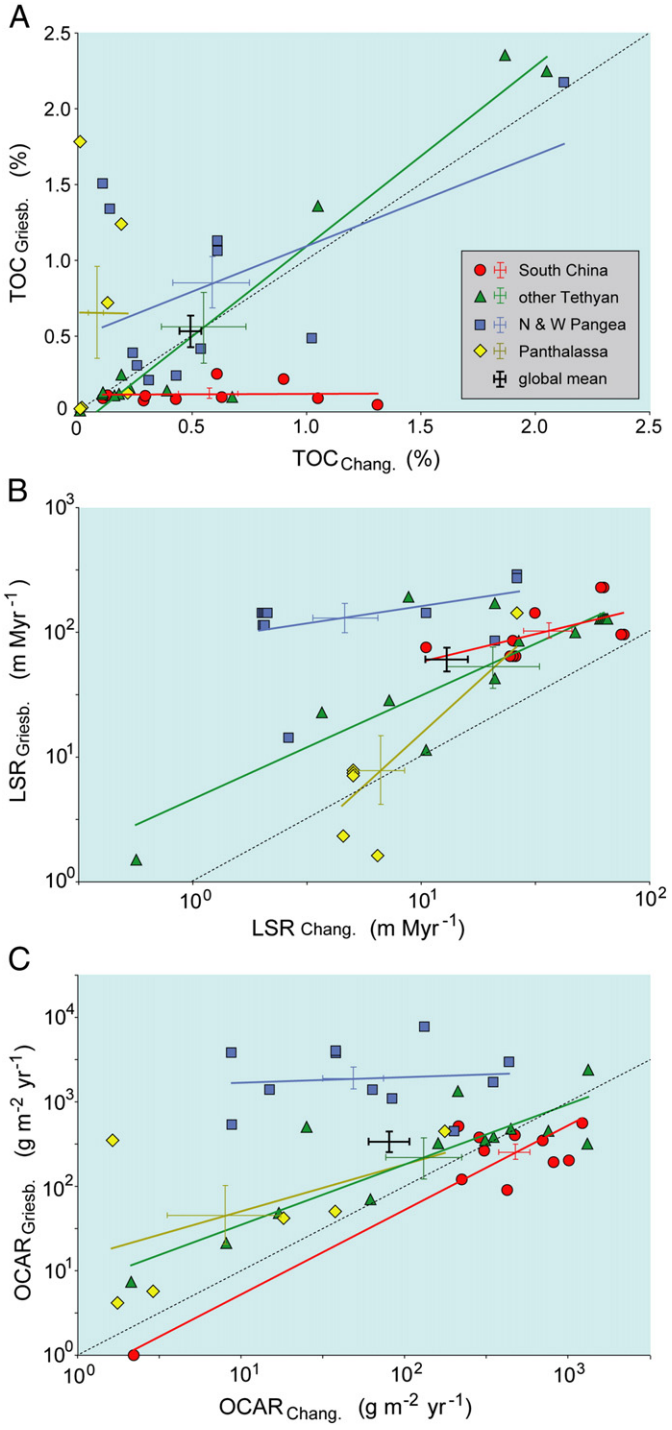

Fig. 7. Crossplots of (A) total organic carbon (TOC), (B) linear sedimentation rate (LSR), and (C) organic carbon accumulation rate (OCAR) for the Changhsingian versus the Griesbachian by study section. Regional groupings of sections indicated by different colors; regional means and ranges of the standard error of the mean shown as colored crosses and global mean as black cross. Solid colored lines represent regressions by region and the dotted black line represents 1:1 parity. Chang. = Changhsingian, Griesb. = Griesbachian. (For interpretation of the references to color in this figure legend, the reader is referred to the web version of this article.)

Differences between the results above and those of Algeo and Twitchett (2010) are due to differences in the durations of time-stratigraphic units. In the present study, the duration of the Changhsingian has been revised downward from 3.4 ± 1.4 Myr to 1.9 ± 0.1 Myr (see Section 2.2), which has resulted in a ~80% increase in all fluxes calculated for the latest Permian as well as a substantial narrowing of their uncertainty limits. The estimated duration of the Griesbachian (0.7 Myr) has not changed although the error range on this estimate has also narrowed considerably. An ~80% increase in Changhsingian fluxes has the effect of reducing the change in mean global LSRs and BARs across the LPME from a factor of ~7× (Algeo and Twitchett, 2010) to one of ~4.5× (present study). Further, the reduced uncertainties of time-stratigraphic unit durations in the present study mean that the flux estimates reported herein are unlikely to require a significant further revision in the future, and that the factor of a ~4.5× increase in LSRs and BARs across the LPME is a real feature of the PTB transition and not an artifact of dating uncertainties.

The four study regions exhibit distinctive patterns of secular variation in OCARs (Fig. 7C). For the Changhsingian, mean OCARs vary by more than 1.5 orders of magnitude in the following sequence: Panthalassa (7.9 ± 6.9 g m^{-2} yr^{-1}), N&W Pangea (48 ± 21 g m^{-2} yr^{-1}), non-Chinese Tethys (97 ± 58 g m^{-2} yr^{-1}), and South China (387 ± 78 g m^{-2} yr^{-1}). For the Griesbachian, mean OCARs vary by more than 1.5 orders of magnitude in the following sequence: Panthalassa (45 ± 40 g m^{-2} yr^{-1}), non-Chinese Tethys (220 ± 103 g m^{-2} yr^{-1}), South China (265 ± 51 g m^{-2} yr^{-1}), and N&W Pangea (1900 ± 520 g m^{-2} yr^{-1}). Mean OCARs increase from the Changhsingian to the Griesbachian by factors of ~2× for the non-Chinese Tethys, ~6× for Panthalassa, and ~40× for N&W Pangea. Within these regions, all sections exhibit an increase in OCAR across the LPME (Fig. 7C), and differences in mean regional values between the Changhsingian and Griesbachian are statistically significant at the 1% level. On the other hand, South China exhibits a *decrease* in mean OCARs from the Changhsingian to the Griesbachian by a factor of ~0.7×. In this region, most sections show a decline in OCAR across the LPME, and the difference between mean OCARs for the Changhsingian and Griesbachian is statistically significant at the 5% level. The mean OCAR of all study sections is greater for the Griesbachian (328 ± 94 g m^{-2} yr^{-1}) than for the Changhsingian (78 ± 25 g m^{-2} yr^{-1}) by a factor of ~4×.

3.3. Pre-burial organic carbon fluxes

The procedure described in Section 2.5 was used to back-calculate OC fluxes at four earlier stages in the depositional history of each study section, prior to (1) late diagenetic OC loss through thermal maturation (f_{OC}'), (2) early diagenetic OC loss through BSR (f_{OC}''), (3) early diagenetic OC loss through aerobic decay (f_{OC}'''), and (4) OC remineralization in the water column (f_{OC}''''; Fig. 4B; Supplement Table 3). Relative to f_{OC} (= OCAR) at Meishan, the resulting estimates for f_{OC}''' (= sinking flux) and f_{OC}'''' (= PPR) are larger by factors of ~7× and 12×, respectively, with estimated uncertainties of about ±2.5× (Fig. 8A). The relatively small multiples for these fluxes relative to OCAR, and the correspondingly large values of BE (=f_{OC}/f_{OC}''', 0.14) and PF (=f_{OC}/f_{OC}'''', 0.08), are a function of low burial temperatures (equivalent to R_o of 0.65%) and shallow depositional water depths

(~30 m), minimizing the scale of corrections for f_{OC}' and f_{OC}'''', respectively. On the other hand, the Gujo-Hachiman section in Japan yields estimates for f_{OC}''' and f_{OC}'''' that are larger than f_{OC} by factors of ~82× and >1000×, and estimates for BE and PF equal to 0.012 and <0.001, respectively (Fig. 8B). Gujo-Hachiman is representative of sections having higher burial temperatures (equivalent to R_o of 4.0–4.5%) and/or greater depositional water depths (3000–5000 m), and that consequently yield much larger flux multiples. The flux estimates for Meishan are probably fairly accurate, but those for Gujo-Hachiman clearly are not and can be viewed only as broadly indicative of the magnitude of OC loss during water-column transit and burial.

Back-calculated OC fluxes largely confirm the secular and regional patterns of variation documented earlier on the basis of OCARs (Fig. 7). First, most South China sections exhibit a pronounced decline in pre-burial OC fluxes from the Changhsingian to the Griesbachian (Fig. 9A and B). On a percentage basis, the declines in these fluxes are even larger than for OCAR (Fig. 9C). As with OCAR, most non-Chinese Tethyan sections exhibit only limited change in pre-burial OC fluxes from the Changhsingian to the Griesbachian, and most N&W Pangean and Panthalassic sections exhibit increased fluxes. Second, regional variation in pre-burial OC fluxes is broadly similar to that in OCAR, although some differences emerge. N&W Pangean and, especially, Panthalassic sections yield larger flux multiples because of the higher burial temperatures (equivalent to R_o of 4.0–4.5%) and/or greater depositional water depths (3000–5000 m) associated with these regions. Thus, although OCARs for sections in these two regions are commonly lower than for Tethyan sections, pre-burial OC fluxes are generally higher (Fig. 9A and B). However, this distinction applies only to absolute OC fluxes and not to relative secular changes (Fig. 9C), which are generally similar for OCAR and pre-burial OC fluxes in all regions because both burial temperature and water depth are general parameters of each study section and do not introduce variance between Changhsingian and Griesbachian flux estimates. Finally, the flux multiples for sections such as Meishan (e.g., <10) are often smaller than the 2 to 3 order-of-magnitude differences in OC fluxes between study sections (spatial variation) and time-stratigraphic units (temporal variation). When pre-burial OC fluxes for a single section exhibit less variance than for the study dataset as a whole, the differences in fluxes among sections is probably real. We conclude that back-calculation of pre-burial OC fluxes does not significantly modify patterns of secular and regional variation shown by OCARs, and that such patterns can generally be recognized by investigation of OCARs.

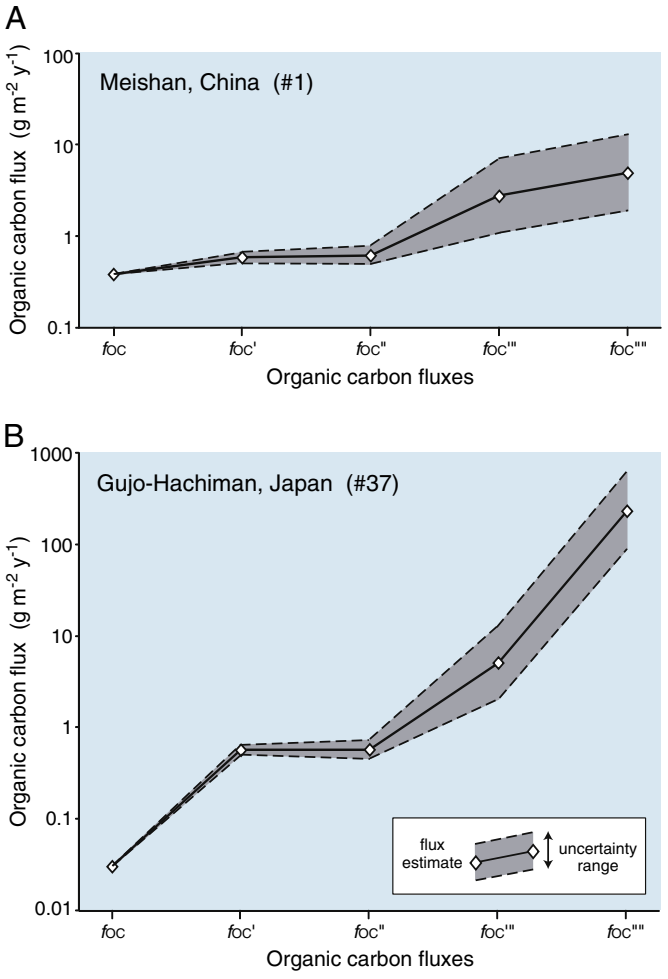

Fig. 8. Examples of back-calculated pre-burial OC fluxes for the Changhsingian of (A) Meishan and (B) Gujo-Hachiman, per Eqs. (4)–(9). Compounded uncertainty ranges are shown by the gray fields bounded by dashed lines. Note that estimated f_{OC}'''' values are <10× greater than f_{OC} for many shallowly buried, shallow-marine sections such as Meishan, but >1000× greater for some deeply buried, deep-marine sections such as Gujo-Hachiman. OC flux estimates for the former sections can be regarded as moderately reliable, whereas those for the latter sections are highly uncertain.

3.4. BAR–OC flux relationships

Relationships between BARs and OCARs can potentially provide insights regarding the accumulation of organic matter in sediments. BAR and OCAR always exhibit a strong positive correlation in sedimentary systems (Middelburg et al., 1997; Tyson, 2005), but different patterns of covariation are observed for oxic versus suboxic–anoxic facies in modern marine systems (Fig. 10). For modern oxic marine facies, BARs and OCARs show a well-defined relationship on a log–log crossplot with a slope of 1.27 (thick solid line, Fig. 10). A slope of >1.0 indicates that OCAR increases more rapidly than BAR: at low BAR (e.g., 1 g m^{-2} yr^{-1}), OCAR averages 0.004 g m^{-2} yr^{-1} (equivalent to a TOC of 0.4%), and at high BAR (e.g., 1000 g m^{-2} yr^{-1}), OCAR averages 25 g m^{-2} yr^{-1} (equivalent to a TOC of 2.5%). Sub/anoxic facies yield higher OCARs for a given BAR but with a lower slope (0.77; thin solid line, Fig. 10). A slope of <1.0 indicates that OCAR increases more slowly than BAR: at low BAR (e.g., 30 g m^{-2} yr^{-1}), OCAR averages 2.1 g m^{-2} yr^{-1} (equivalent to a TOC of 7.0%), and at high BAR (e.g., 1000 g m^{-2} yr^{-1}), OCAR averages 30 g m^{-2} yr^{-1} (equivalent to a TOC of 3.0%). The oxic and sub/anoxic trends show maximal differences in OCARs at low BARs because preservation of organic matter in sediments is most strongly enhanced by the absence of dissolved oxygen where sedimentation rates are lowest. Conversely, the oxic and sub/anoxic trends converge at high BARs because organic matter is buried rapidly in both facies and, hence, tends to be well-preserved regardless of the redox conditions at the SWI.

For PTB sections of the present study, OCAR (f_{OC}) increases with increasing BAR (Fig. 10A). Non-Chinese sections exhibit large Changhsingian-to-Griesbachian increases in both BARs (factor of ~6×) and OCARs (factor of ~8×), defining a trend with a slope of 1.25 (dashed line) that is parallel to but offset from the modern oxic marine facies trend by −0.72 log units (equivalent to a factor of 0.2×). Thus, non-Chinese sections exhibit OCARs that are, on average, just 20% of that for modern facies at a given BAR, a difference attributable to OC loss during diagenesis. Back-calculated OC sinking fluxes (f_{OC}''') yield a nearly identical regression relationship to that of OCARs for modern oxic facies (Fig. 10B), presumably because the modern marine values represent measurements at shallow burial depths prior to significant diagenetic loss of OC. The observation that OC fluxes for PTB sections more closely model the modern marine trend for oxic facies than for sub/anoxic facies (despite a few outliers within the sub/anoxic field) is consistent with the hypothesis that Late Permian–Early Triassic shallow-marine environments were

Please cite this article as: Algeo, T.J., et al., Plankton and productivity during the Permian–Triassic boundary crisis: An analysis of organic carbon fluxes, Glob. Planet. Change (2012), doi:10.1016/j.gloplacha.2012.02.008

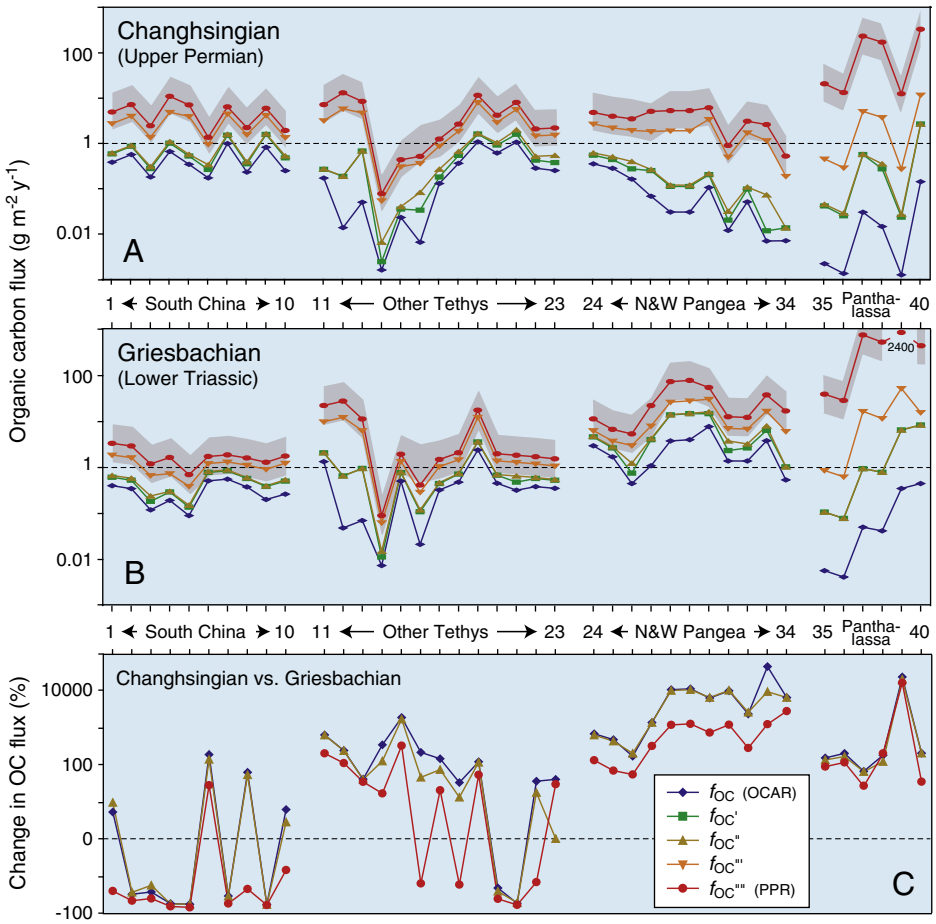

Fig. 9. Back-calculated pre-burial OC fluxes arranged by geographic region (see Supplement Table 1 for section numbers): (A) Changhsingian, (B) Griesbachian, and (C) difference between the Griesbachian and Changhsingian (in percent). In A and B, the gray fields represent the uncertainty range for estimates of f_{OC}'''' (cf. Fig. 8). In C, no curves are shown for f_{OC}' (identical to f_{OC}) and fOC''' (identical to f_{OC}'''') because thermal maturity (Eq. (4)) and water depth (Eq. (9)) are general parameters of each study section and result in no secular difference in OC flux estimates for the Changhsingian versus Griesbachian (cf. Fig. 5). Horizontal dashed lines in A and B are for reference only; dashed line in C represents zero change. Data given in Supplement Table 3.

well-oxygenated most of the time and experienced only brief episodes of anoxia (Algeo et al., 2007, 2008).

Whereas OCARs and BARs both generally increase across the LPME in non-Chinese sections, South China sections exhibit a 33% *decrease* in OCARs (Fig. 10A) and OC sinking fluxes (Fig. 10B) despite a factor of ~3× increase in BARs. As a consequence, South China Griesbachian units *as a group* (rather than as just a few outliers) plot distinctly below the regression lines for both modern oxic marine facies and non-Chinese PTB units (Fig. 10). Although South China units of both Changhsingian and Griesbachian ages exhibit higher mean BARs than most non-Chinese sections, the range of BARs for South China sections is roughly the same as that for the dozen or so non-Chinese sections with high BARs, the majority of which exhibit much higher OCARs and OC sinking fluxes than the South China sections. These observations emphasize the anomalously low OCARs and pre-burial OC fluxes associated with the Lower Triassic of the South China region (see Sections 3.2 and 3.3).

3.5. Burial efficiencies, preservation factors, and primary productivity rates

Modern marine systems exhibit a well-defined positive relationship between BAR and BE (Tyson, 2005). Higher BAR favors preservation of a larger fraction of organic matter reaching the SWI owing to its reduced time in residence in the zone of aerobic decay. BE increases rapidly in the mid-range of BAR values (~10–100 g m^{-2} yr^{-1}) and asymptotically approaches 100% at BAR > 100 g m^{-2} yr^{-1} (Fig. 11A). Comparison of the modern marine trend with BAR–BE data for PTB sections offers a mechanism for evaluating the accuracy of back-calculated pre-burial OC fluxes for the latter. PTB sections largely overlap the data field for modern marine sediments, tracing out a similar sigmoidal distribution pattern (Fig. 11A; cf. Dunne et al., 2005). This relationship suggests that estimates of f_{OC}''' and BE for the study sections are fairly accurate. A minority of PTB sections exhibit BEs lower than predicted by the modern marine trend, possibly because diagenetic loss of OC has been somewhat overestimated, although the lower BEs may be consistent with the comparatively greater maturity of these sections. No spatial (inter-regional) or temporal (Changshingian-versus-Griesbachian) biases are evident in BE estimates.

Modern marine systems also exhibit a well-defined positive relationship between BAR and PF due to better preservation of organic matter at higher BARs (Tyson, 2005). For a given BAR, PFs are higher in sub/anoxic facies (trend II) than in oxic facies (trend I; Fig. 11B). PTB sections yield systematically higher PFs than either oxic or sub/anoxic facies in modern marine systems. The PTB units appear to parallel the sub/anoxic trend more closely, from which might be inferred that redox conditions in PTB marine systems were predominantly suboxic or anoxic. However, this inference conflicts with the inference of mainly oxic conditions based on BAR–OCAR relationships (see Section 3.4). Our preferred interpretation is that f_{OC}'''' and PF have been systematically underestimated for PTB sections, probably by an average factor of 3–10×. This interpretation is consistent with differences in estimated PPRs for PTB sections, which are mostly <10 g C m^{-2} yr^{-1} (Fig. 9A and B), and measured PPRs for modern

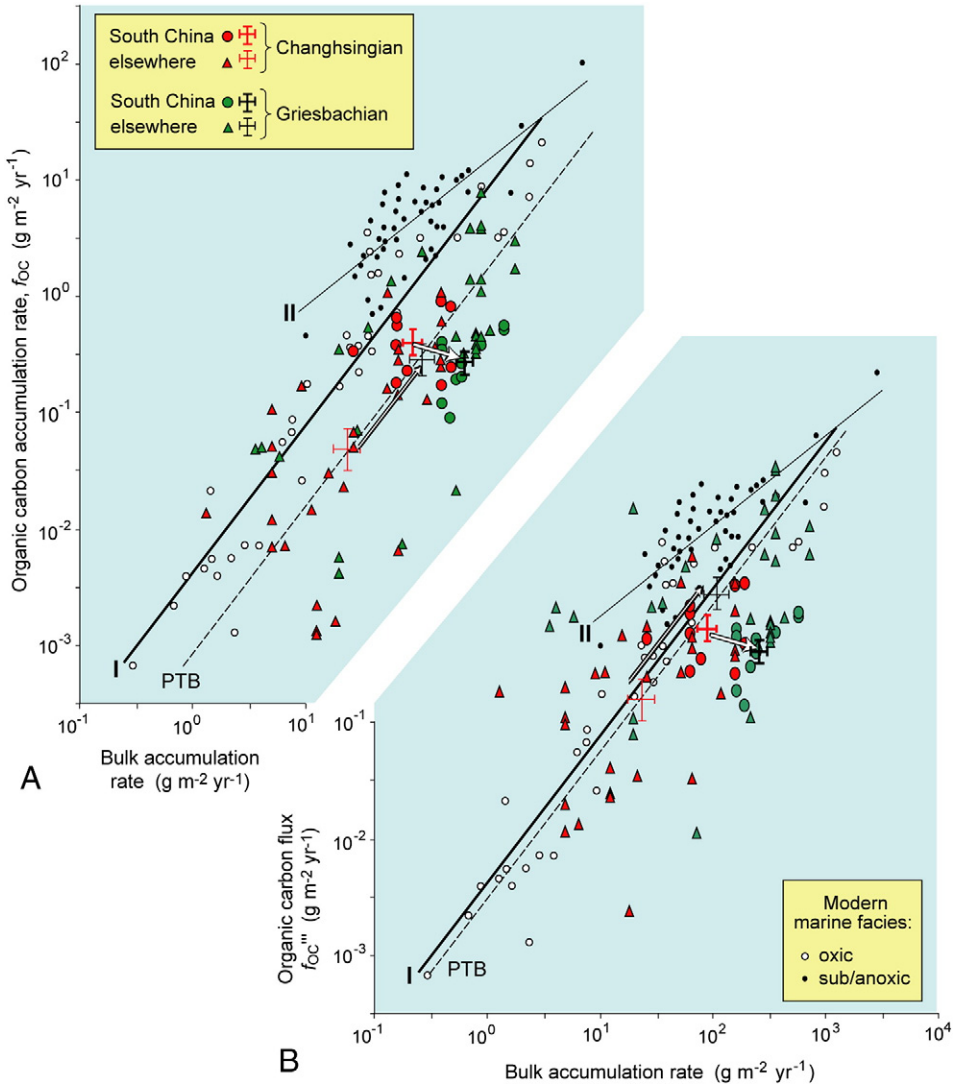

Fig. 10. BAR versus OC flux: f_{OC} (A) and f_{OC}''' (B). Modern marine data from Tyson (2005); oxic facies = white symbols, regression line I; sub/anoxic facies = black symbols, regression line II. PTB sections = colored symbols, dashed regression line (for non-Chinese sections only); in order to emphasize contrasts with South China, sections from other regions have been pooled; for each region, the means and ranges of the standard error of the mean are shown as colored crosses; white arrows show patterns of Changhsingian-to-Griesbachian change for South China and non-Chinese sections. See text for discussion. (For interpretation of the references to color in this figure legend, the reader is referred to the web version of this article.)

marine systems, which range from ~25–50 g C m^{-2} yr^{-1} in low-productivity zones of the open ocean to 250–350 g C m^{-2} yr^{-1} in high-productivity upwelling zones (Meyers, 1997; Nelson et al., 2002; n.b. new satellite-based estimates are higher, ~500–1000 g C m^{-2} yr^{-1}, e.g., Behrenfeld et al., 2005; Patti et al., 2008). This discrepancy presumably reflects our inability to accurately back-calculate f_{OC}'''' and underscores the need to view PPR estimates for paleomarine systems with caution.

4. Discussion

4.1. Potential influences on OC flux patterns

Although many potential influences on OC fluxes exist in the marine environment, most of these factors were probably insufficient to have been the principal cause of the regional and secular anomalies in OC fluxes documented in this study. First, sedimentary facies can exert influences on organic matter preservation through particle-size and permeability effects, e.g., fine-grained shale is inherently prone to higher TOC values than coarser siliciclastic facies owing to greater particulate surface area (Kennedy et al., 2002; Kennedy and Wagner, 2011), charge imbalances on the surfaces of clay minerals (Ohashi and Nakazawa, 1996), and reduced permeability (Rothman and Forney, 2007). Almost all PTB sections exhibit a shift toward more clay-rich compositions from the Changhsingian to the Griesbachian (Algeo and Twitchett, 2010, their Fig. 3), a condition that should have enhanced the preservation of organic matter (Kennedy et al., 2002; Rothman and Forney, 2007). Second, rapid sedimentation enhances the preservation of organic matter in sediments (Fig. 10; Canfield, 1994; Tyson, 2005; Dunne et al., 2007). Almost all PTB sections exhibit an increase in LSRs and BARs from the Changhsingian to the Griesbachian (Fig. 7B). Third, benthic redox conditions influence OC fluxes, with anoxic conditions favoring higher BEs and PFs (Fig. 11; Canfield, 1994; Tyson, 2005). Many PTB sections have yielded evidence of intensified anoxia during the latest Permian (post-LPME) and Early Triassic (Nielsen and Shen, 2004; Grice et al., 2005; Riccardi et al., 2006; Hays et al., 2007; Algeo et al., 2007, 2008, 2010, 2011b; Cao et al., 2009; Bond and Wignall, 2010), although, as argued above, the integrated intensity of redox changes may have been limited in shallow-marine settings.

Please cite this article as: Algeo, T.J., et al., Plankton and productivity during the Permian–Triassic boundary crisis: An analysis of organic carbon fluxes, Glob. Planet. Change (2012), doi:10.1016/j.gloplacha.2012.02.008

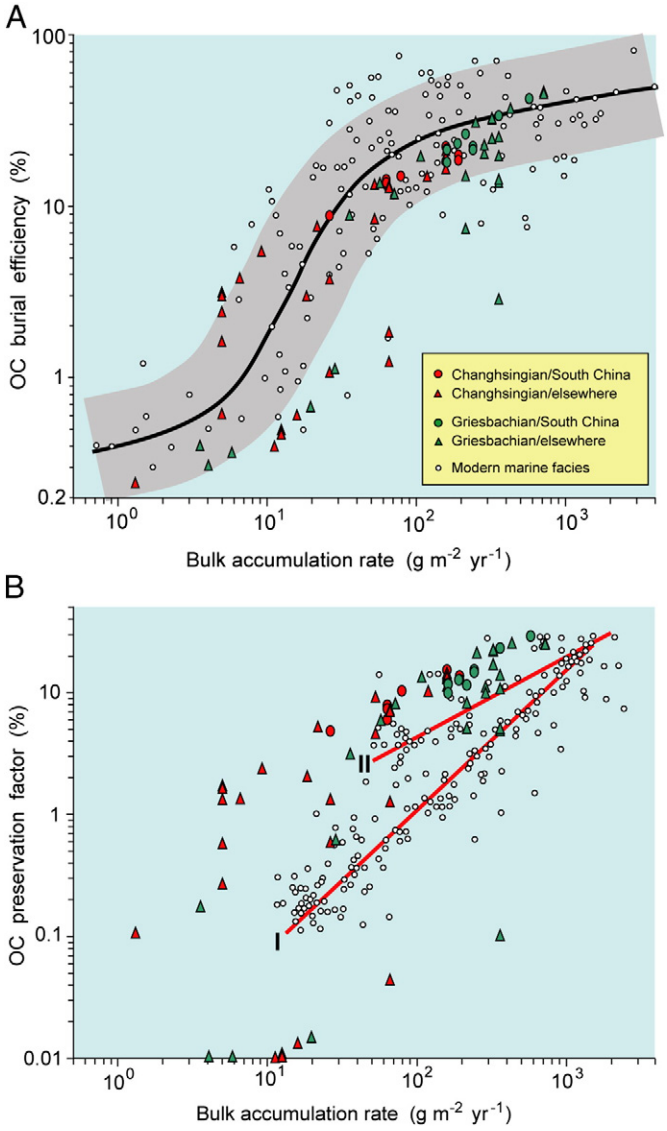

Fig. 11. BAR versus (A) burial efficiency (BE), and (B) preservation factor (PF). Modern marine sediments shown as white symbols and PTB sections as colored symbols. In A, the modern marine trend is shown by the black line and gray field; in B, trends I and II represent oxic and sub/anoxic facies, respectively. Note that PTB sections bracket the modern marine trend in A, suggesting that estimates of f_{OC}'' and BE are probably fairly accurate; however, PTB sections plot systematically higher than the modern data field in B, suggesting that f_{OC}'''' and PF have been systematically underestimated. (For interpretation of the references to color in this figure legend, the reader is referred to the web version of this article.)

All three of the factors above should have favored enhanced OC preservation in Griesbachian sediments and, indeed, may have contributed to higher OC fluxes in non-Chinese sections (Fig. 7C). However, these factors cannot account for the reduced OC fluxes observed in most South China sections. Indeed, because each of these factors should have favored higher BEs and PFs, actual reductions in PPRs and OC sinking fluxes in the South China region during the Early Triassic may have been even larger than estimated here. Other influences, e.g., eustatic and tectonic controls, are also unlikely to account for OC flux anomalies in South China PTB sections (see Supplement Section 3 for a fuller discussion). Finally, the uncertainties in the durations of the time-stratigraphic units of the present study are too small (±5–10%; see Section 2.2) to account for the OC flux anomalies.

4.2. A marine productivity crash in the South China region?

The contrast in secular variation of OC fluxes between PTB sections in South China and those elsewhere is striking. Although a few non-Chinese sections show declines across the LPME, no region except South China exhibits such an abrupt or widespread decrease in OC fluxes (see Sections 3.3 and 3.4). Because this pattern cannot be accounted for through secular changes in sedimentation rates, depositional facies, redox conditions, or other variables (see Section 4.1), we infer a catastrophic "crash" in marine primary productivity across the South China region at the time of the LPME. The magnitude of this decline was ~80% of pre-LPME productivity (or possibly more, if other factors influencing PF are considered; see Section 4.1), an estimate consistent with reported decreases in radiolarian productivity in the South China region (Shen et al., 2012). Based on TOC profiles (Fig. 6A), it appears that the onset of the productivity crash at the LPME was fairly abrupt, and that productivity remained low for an extended interval (at least several 100 kyr) thereafter.

The causes of the marine productivity crash in the South China region are uncertain, although oceanographic factors are likely to have played a major role. A study of a PTB section at Nhi Tao, Vietnam demonstrated that this shallow-marine carbonate platform experienced at least 9 incursions of sulfidic deepwaters beginning at the LPME and continuing at intervals for 100(+)kyr into the Early Triassic (Algeo et al., 2007, 2008). The exact concurrence in timing between the LPME, the appearance of ^{34}S-depleted pyrite framboid layers, and an abrupt decline in TOC values to near zero is an indication that sulfide poisoning was the likely cause of both the marine productivity crash and the mass extinction of shallow-marine benthic organisms, at least in the Nanpanjiang Basin region. The mechanism of deepwater incursion might have been either localized upwelling or a more widespread rise of the chemocline, possibly leading to eruptions of H_2S into the ocean-surface layer and atmosphere (Kump et al., 2005). The observation that incursions of sulfidic waters occurred repeatedly (Algeo et al., 2007, 2008) suggests a possible cause for the delayed recovery of benthic shallow-marine communities during the Early Triassic (Payne et al., 2006; Bottjer et al., 2008). A recent study argued on the basis of water-column $\delta^{13}C$ gradients that marine primary productivity increased rather than decreased in the South China region during the Early Triassic (Meyer et al., 2011). However, a reanalysis based on a spatially and bathymetrically broader dataset demonstrated that the Early Triassic steepening of vertical $\delta^{13}C$ gradients in South China seas was due mainly to intensified water-column stratification rather than to enhanced marine productivity (Song et al., this volume) and, hence, is not at odds with the conclusions of the present study.

The possibility that the marine productivity crash was caused by volcanism warrants consideration given the close association between the LPME and volcanic ash layers in South China PTB sections. Although the eruption of the Siberian Traps was the likely trigger for the LPME (Reichow et al., 2009), it is difficult to envision how this event could have been responsible for marine environmental changes in South China without producing similar effects over a broader area of the globe (Fig. 2A). The South China region itself was volcanically active during the Permian–Triassic transition, as shown by volcanic ash layers in many sections (Yin et al., 1992; Feng et al., 2007; Tong et al., 2007; Xie et al., 2010; Shen et al., 2012), including the "boundary clay" of Bed 25 at Meishan (Yin et al., 2001; Xu et al., 2007). These volcanic ash layers are thought to have been generated in a subduction-zone volcanic arc along the South China–Indochina plate margin (Fig. 2B). Large volcanic eruptions can be detrimental to marine life in various ways, as shown at a small scale by the 1991 eruption of Mount Pinatubo in the Philippines, which deposited an ash layer across the South China Sea that thinned from ~10 cm to a feather edge distally (Wiesner et al., 1995). The ash layer prevented vertical migration of benthic taxa as well as the downward diffusion of

Please cite this article as: Algeo, T.J., et al., Plankton and productivity during the Permian–Triassic boundary crisis: An analysis of organic carbon fluxes, Glob. Planet. Change (2012), doi:10.1016/j.gloplacha.2012.02.008

dissolved oxygen, thus inducing porewater anoxia at shallow depths and causing steep declines in foraminifer abundance and diversity (Hess and Kuhnt, 1996; Haeckel et al., 2001; Kuhnt et al., 2005). The effects of volcanism on marine plankton are more poorly known: volcanic ash might be either helpful through fertilization effects (Frogner et al., 2001) or harmful through reduction of light penetration, deposition of toxic trace metals, and acidification of surface waters (Felitsyn and Kirianov, 2002; Sansone et al., 2002; Paytan et al., 2009). The main difficulty in evoking a volcanic mechanism as the cause of the productivity crash in South China PTB sections is that the effects of such an event should have dissipated rapidly, yet (as noted above) low levels of productivity persisted for at least several 100 kyr following the LPME.

4.3. Enhanced primary productivity in the Early Triassic ocean?

Although the positive covariation between OC fluxes and BARs in non-Chinese PTB sections (Fig. 10) is likely to have been controlled principally by sedimentation rate influences on organic matter preservation (see Section 3.5), the possibility that Early Triassic marine primary productivity were generally elevated should not be dismissed. Elevated primary productivity rates during the Early Triassic have been inferred recently on the basis of (1) rapid expansion of the oceanic oxygen-minimum zone at the LPME (Algeo et al., 2010, 2011b), and (2) large shallow-to-deep C-isotopic gradients (Meyer et al., 2011; Song et al., this volume). A possible trigger for productivity increases was a major soil erosion event that occurred just prior to the LPME (Ward et al., 2000; Retallack, 2005; Sephton et al., 2005; Xie et al., 2005, 2007; Wang and Visscher, 2007), which was followed by sustained high rates of chemical weathering in land areas during the Early Triassic (Sheldon, 2006; Algeo and Twitchett, 2010). These events would have liberated essential nutrients (especially N and P) from soils and bedrock and transferred them to marine ecosystems via river runoff (Fig. 1B; cf. Algeo et al., 1995, 2001). Elevated nutrient inventories in ocean-surface waters stimulated primary productivity and triggered changes in phytoplankton community composition favoring taxa better adapted to eutrophic conditions (see Section 1; Algeo et al., 2011a). Similar effects have been observed in modern marine systems subject to elevated fluxes of anthropogenic nutrients (Helly and Levin, 2004; Diaz and Rosenberg, 2008). Elevated nutrient levels and enhanced primary productivity may have been a contributing factor to the widespread development of oceanic anoxia at the PTB (Fig. 1B; cf. Winguth and Maier-Reimer, 2005; Meyer et al., 2008). However, these effects may have been relatively short-lived (<100 kyr?), as marine productivity rates appear to have declined during the Early Triassic in some regions, such as the Canadian Western Sedimentary Basin (Schoepfer et al., 2012).

5. Conclusions

PTB sections from South China exhibit abrupt declines in TOC and OCAR from the Changhsingian (latest Permian) to the Griesbachian (earliest Triassic), a pattern not observed for sections in other regions. This pattern cannot be explained through secular changes in sedimentation rates, sedimentary facies, or redox conditions, all of which would have favored higher TOCs and OCARs during the Griesbachian, nor can it be accounted for through loss of OC during transit in the water column or diagenesis in the sediment. The most likely explanation is a collapse of marine primary productivity across the South China region that commenced at the LPME and continued for hundreds of thousands of years into the Early Triassic. This productivity crash and the concurrent extinctions among the benthic marine fauna coincided with the deposition of the "boundary clay" at Meishan D, an association that suggests that a major explosive volcanic eruption of uncertain provenance triggered the PTB crisis. In other PTB sections globally, OCARs increased on average by a factor of ~4× across the LPME, largely as a function of a concurrent increase in BARs. Increasing BARs during the Early Triassic were probably due to elevated rates of subaerial weathering and fluxes of detrital material to shallow-marine systems. Intensification of chemical weathering relative to physical weathering is likely to have increased the flux of nutrients to the Early Triassic ocean, leading to an increase in marine productivity that may have contributed to the development of widespread marine anoxia.

Acknowledgments

Thanks to Rick Morante and Kliti Grice for unpublished TOC data from East Greenland and to Roger Summons for helpful discussions. Thanks to Michael Brookfield, Brooks Ellwood, Micha Horacek, Leo Krystyn, Richard Twitchett, and Paul Wignall for samples from various PTB sections. This project was supported in part by grants to TJA from the National Science Foundation (EAR-0618003, EAR-0745574, and EAR-1053449), to CMH from the Natural Sciences and Engineering Research Council of Canada Discovery Grant program, and to JNT from the National Science Foundation of China (NSFC project no. 40830212). This paper is a contribution to IGCP Project 572.

Appendix A. Supplementary data

Supplementary data to this article can be found online at doi:10.1016/j.gloplacha.2012.02.008.

References

Algeo, T., Twitchett, R., 2010. Anomalous Early Triassic sediment fluxes due to elevated weathering rates and their biological consequences. Geology 38, 1023–1026.
Algeo, T.J., Berner, R.A., Maynard, J.B., Scheckler, S.E., 1995. Late Devonian oceanic anoxic events and biotic crises: "rooted" in the evolution of vascular land plants? GSA Today 5, 45, 64–66.
Algeo, T.J., Scheckler, S.E., Maynard, J.B., 2001. Effects of early vascular land plants on weathering processes and global chemical fluxes during the Middle and Late Devonian. In: Gensel, P., Edwards, D. (Eds.), Plants Invade the Land: Evolutionary and Environmental Perspectives. Columbia University Press, New York, pp. 213–236.
Algeo, T.J., Ellwood, B.B., Nguyen, T.K.T., Rowe, H., Maynard, J.B., 2007. The Permian–Triassic boundary at Nhi Tao, Vietnam: evidence for recurrent influx of sulfidic watermasses to a shallow-marine carbonate platform. Palaeogeography, Palaeoclimatology, Palaeoecology 252, 304–327.
Algeo, T.J., Shen, Y., Zhang, T., Lyons, T.W., Bates, S.M., Rowe, H., Nguyen, T.K.T., 2008. Association of ^{34}S-depleted pyrite layers with negative carbonate δ^{13}C excursions at the Permian/Triassic boundary: evidence for upwelling of sulfidic deep-ocean watermasses. Geochemistry, Geophysics, Geosystems 9, Q04025 (10 pp.).
Algeo, T.J., Hinnov, L., Moser, J., Maynard, J.B., Elswick, E., Kuwahara, K., Sano, H., 2010. Changes in productivity and redox conditions in the Panthalassic Ocean during the latest Permian. Geology 38, 187–190.
Algeo, T.J., Chen, Z.Q., Fraiser, M.L., Twitchett, R.J., 2011a. Terrestrial–marine teleconnections in the collapse and rebuilding of Early Triassic marine ecosystems. Palaeogeography, Palaeoclimatology, Palaeoecology 308, 1–11.
Algeo, T.J., Kuwahara, K., Sano, H., Bates, S., Lyons, T., Elswick, E., Hinnov, L., Ellwood, B.B., Moser, J., Maynard, J.B., 2011b. Spatial variation in sediment fluxes, redox conditions, and productivity in the Permian–Triassic Panthalassic Ocean. Palaeogeography, Palaeoclimatology, Palaeoecology 308, 65–83.
Algeo, T., Henderson, C., Ellwood, B., Rowe, H., Elswick, E., Bates, S., Lyons, T., Hower, J.C., Smith, C., Maynard, J.B., Hays, L., Summons, R., Fulton, J., Freeman, K., 2012. Evidence for a diachronous Late Permian marine crisis from the Canadian Arctic region. Geological Society of America Bulletin. doi:10.1130/B30505.1 (publ. online 6 February 2012).
Ando, A., Kodama, K., Kojima, S., 2001. Low-latitude and Southern Hemisphere origin of Anisian (Triassic) bedded chert in the Inuyama area, Mino terrane, central Japan. Journal of Geophysical Research 106 (B2), 1973–1986.
Bao, Z., 1998. Continental slope limestones of Lower and Middle Triassic, South China. Sedimentary Geology 118, 77–93.
Behrenfeld, M.J., Boss, E., Siegel, D.A., Shea, D.M., 2005. Carbon-based ocean productivity and phytoplankton physiology from space. Global Biogeochemical Cycles 19, GB1006 (14 pp.).
Benning, L.G., Wilkin, R.T., Barnes, H.L., 2000. Reaction pathways in the Fe–S system below 100 °C. Chemical Geology 167, 25–51.
Berner, R.A., 1970. Sedimentary pyrite formation. American Journal of Science 268, 1–23.
Berner, R.A., 1978. Sulfate reduction and the rate of deposition of marine sediments. Earth and Planetary Science Letters 37, 492–498.
Berner, R.A., 1984. Sedimentary pyrite formation: an update. Geochimica et Cosmochimica Acta 48, 605–615.

Berner, R.A., 2002. Examination of hypotheses for the Permo-Triassic boundary extinction by carbon cycle modeling. Proceedings of the National Academy of Sciences of the United States of America 99, 4172–4177.
Bertrand, P., Lallier-Vergès, E., 1993. Past sedimentary organic matter accumulation and degradation controlled by productivity. Nature 364, 786–788.
Bishop, J.K.B., 1989. Regional extremes in particulate matter composition and flux: effects on the chemistry of the ocean interior. In: Berger, W.H., Smetacek, V.S., Wefer, G. (Eds.), Productivity of the Ocean: Present and Past. Wiley & Sons, Chichester, pp. 117–137.
Bond, D.P.G., Wignall, P.B., 2010. Pyrite framboid study of marine Permian–Triassic boundary sections: a complex anoxic event and its relationship to contemporaneous mass extinction. Geological Society of America Bulletin 122, 1265–1279.
Bottjer, D.J., Clapham, M.E., Frasier, M.L., Powers, C.M., 2008. Understanding mechanisms for the end-Permian mass extinction and the protracted Early Triassic aftermath and recovery. GSA Today 18, 4–10.
Bowring, S.A., Erwin, D.H., Jin, Y.G., Martin, M.W., Davidek, K., Wang, W., 1998. U/Pb zircon geochronology and tempo of the end-Permian mass extinction. Science 280, 1039–1045.
Bralower, T.J., Thierstein, H.R., 1984. Low productivity and slow deep-water circulation in mid-Cretaceous oceans. Geology 12, 614–618.
Brennecka, G.A., Herrmann, A.D., Algeo, T.J., Anbar, A.D., 2011. Rapid expansion of oceanic anoxia immediately before the end-Permian mass extinction. Proceedings of the National Academy of Sciences of the United States of America 108, 17631–17634.
Canfield, D.E., 1994. Factors influencing organic carbon preservation in marine sediments. Chemical Geology 114, 315–329.
Cao, C., Hays, L.E., Love, G.D., Bowring, S.A., Wang, W., Shen, S., Summons, R.E., 2009. Biogeochemical evidence for euxinic oceans and ecological disturbance presaging the end-Permian mass extinction event. Earth and Planetary Science Letters 281, 188–201.
Caplan, M.L., Bustin, R.M., 1999. Devonian–Carboniferous Hangenberg mass extinction event, widespread organic-rich mudrock and anoxia; causes and consequences. Palaeogeography, Palaeoclimatology, Palaeoecology 148, 187–207.
Cramer, B.D., Saltzman, M.R., 2005. Sequestration of ^{12}C in the deep ocean during the early Wenlock (Silurian) positive carbon isotope excursion. Palaeogeography, Palaeoclimatology, Palaeoecology 219, 333–349.
Czamanske, G.K., Gurevitch, A.B., Fedorenko, V., Simonov, O., 1998. Demise of the Siberian plume: paleogeographic and paleotectonic reconstruction from the prevolcanic and volcanic record, north-central Siberia. International Geology Review 40, 95–115.
Diaz, R.J., Rosenberg, R., 2008. Spreading dead zones and consequences for marine ecosystems. Science 321, 926–929.
Dunne, J.P., Armstrong, R.A., Gnanadesikan, A., Sarmiento, J.L., 2005. Empirical and mechanistic models for the particle export ratio. Global Biogeochemical Cycles 19, GB4026.
Dunne, J.P., Sarmiento, J.L., Gnanadesikan, A., 2007. A synthesis of global particle export from the surface ocean and cycling through the ocean interior and on the seafloor. Global Biogeochemical Cycles 21, GB4006 (16 pp.).
Erwin, D.H., Bowring, S.A., Jin, Y.-G., 2002. End-Permian mass-extinctions: a review. In: Koeberl, C., MacLeod, K.G. (Eds.), Catastrophic Events and Mass Extinctions: Impacts and Beyond: Geological Society of America Special Paper, 356, pp. 353–383.
Felitsyn, S.B., Kirianov, V.Y., 2002. Mobility of phosphorus during the weathering of volcanic ashes. Lithology and Mineral Resources 37, 275–278.
Feng, Q., He, W., Gu, S., Meng, Y., Jin, Y., Zhang, F., 2007. Radiolarian evolution during the latest Permian in South China. Global and Planetary Change 55, 177–192.
Frogner, P., Gíslason, S.R., Óskarsson, N., 2001. Fertilizing potential of volcanic ash in ocean surface water. Geology 29, 487–490.
Galfetti, T., Bucher, H., Ovtcharova, M., Schaltegger, U., Brayard, A., Brühwiler, T., Goudemand, N., Weissert, H., Hochuli, P.A., Cordey, F., Guodun, K., 2007. Timing of the Early Triassic carbon cycle perturbations inferred from new U–Pb ages and ammonoid biochronozones. Earth and Planetary Science Letters 258, 593–604.
Grice, K., Cao, C., Love, G.D., Böttcher, M.E., Twitchett, R.J., Grosjean, E., Summons, R.E., Turgeon, S.C., Dunning, W., Jin, Y., 2005. Photic zone euxinia during the Permian–Triassic superanoxic event. Science 307, 706–709.
Guo, G., Tong, J., Zhang, S., Zhang, J., Bai, L., 2008. Cyclostratigraphy of the Induan (Early Triassic) in West Pingdingshan Section, Chaohu, Anhui Province. Science in China Series D: Earth Sciences 51, 22–29.
Gupta, L.P., Kawahata, H., 2006. Downcore diagenetic changes in organic matter and implications for paleoproductivity estimates. Global and Planetary Change 53, 122–136.
Haeckel, M., van Beusekom, J., Wiesner, M.G., König, I., 2001. The impact of the 1991 Mount Pinatubo tephra fallout on the geochemical environment of the deep-sea sediments in the South China Sea. Earth and Planetary Science Letters 193, 151–166.
Hays, L.E., Beatty, T., Henderson, C.M., Love, G.D., Summons, R.E., 2007. Evidence for photic zone euxinia through the end-Permian mass extinction in the Panthalassic Ocean (Peace River Basin, Western Canada). Palaeoworld 16, 39–50.
Hedges, J.I., Clark, W.A., Cowie, G.L., 1988. Fluxes and reactivities of organic matter in a coastal marine bay. Limnology and Oceanography 33, 1137–1152.
Helly, J.J., Levin, L.A., 2004. Global distribution of naturally occurring marine hypoxia on continental margins. Deep-Sea Research I 51, 1159–1168.
Henderson, C.M., 1997. Uppermost Permian conodonts and the Permian–Triassic boundary in the Western Canada Sedimentary Basin. Bulletin of Canadian Petroleum Geology 45, 693–707.
Henderson, C.M., Mei, S.L., 2007. Geographical clines in Permian and lower Triassic gondolellids and its role in taxonomy. Palaeoworld 16, 190–201.
Henrichs, S.M., Reeburgh, W.S., 1987. Anaerobic mineralization of marine sediment organic matter; rates and the role of anaerobic processes in the oceanic carbon economy. Geomicrobiology Journal 5, 191–237.
Hess, S., Kuhnt, W., 1996. Deep-sea benthic foraminiferal recolonization of the 1991 Mt. Pinatubo ash layer in the South China Sea. Marine Micropaleontology 28, 171–197.
Horita, J., Zimmermann, H., Holland, H.D., 2002. Chemical evolution of seawater during the Phanerozoic: implications from the record of marine evaporites. Geochimica et Cosmochimica Acta 66, 3733–3756.
Hotinski, R.M., Bice, K.L., Kump, L.R., Najjar, R.G., Arthur, M.A., 2001. Ocean stagnation and end-Permian anoxia. Geology 29, 7–10.
Hunt, J.M., 1996. Petroleum Geochemistry and Geology, 2nd ed. W.H. Freeman, New York. (743 pp.).
Irmis, R.B., Whiteside, J.H., 2011. Delayed recovery of non-marine tetrapods after the end-Permian mass extinction tracks global carbon cycle. Proceedings of the Royal Society B. doi:10/1098/rspb.2011.1895, 9 pp.
Isozaki, Y., 1997. Permo-Triassic boundary superanoxia and stratified superocean; records from lost deep sea. Science 276, 235–238.
Jin, Y.G., Wang, Y., Henderson, C.M., Wardlaw, B.R., Shen, S.Z., Cao, C.Q., 2006. The Global Stratotype Section and Point (GSSP) for the base of the Changhsingian Stage (Upper Permian). Episodes 29, 175–182.
Kennedy, M.J., Wagner, T., 2011. Clay mineral continental amplifier for marine carbon sequestration in a greenhouse ocean. Proceedings of the National Academy of Sciences of the United States of America 108, 9776–9781.
Kennedy, M.J., Hill, R.J., Pevear, D.R., 2002. Mineral surface control of organic carbon in black shale. Science 295, 657–660.
Knoll, A.H., Bambach, R.K., Payne, J.L., Pruss, S., Fischer, W.W., 2007. Paleophysiology and end-Permian mass extinction. Earth and Planetary Science Letters 256, 295–313.
Kuhnt, W., Hess, S., Holbourn, A., Paulsen, H., Salomon, B., 2005. The impact of the 1991 Mt. Pinatubo eruption on deep-sea foraminiferal communities: a model for the Cretaceous–Tertiary (K/T) boundary? Palaeogeography, Palaeoclimatology, Palaeoecology 224, 83–107.
Kump, L.R., Pavlov, A., Arthur, M.A., 2005. Massive release of hydrogen sulfide to the surface ocean and atmosphere during intervals of oceanic anoxia. Geology 33, 397–400.
Kuwahara, K., Yao, A., Yamakita, S., 1998. Reexamination of Upper Permian radiolarian biostratigraphy. Earth Science (Chikyu Kagaku) 52, 391–404 (in Japanese).
Lopes, C., Mix, A.C., Abrantes, F., 2010. Environmental controls of diatom species in Northeast Pacific sediments. Palaeogeography, Palaeoclimatology, Palaeoecology 297, 188–200.
Lowenstein, T.K., Timofeeff, M.N., Kovalevych, V.M., Horita, J., 2005. The major-ion composition of Permian seawater. Geochimica et Cosmochimica Acta 69, 1701–1719.
Luo, G., Kump, L.R., Wang, Y., Tong, J., Arthur, M.A., Yang, H., Huang, J., Yin, H., Xie, S., 2010. Isotopic evidence for an anomalously low oceanic sulfate concentration following end-Permian mass extinction. Earth and Planetary Science Letters 300, 101–111.
Luo, G., Wang, Y., Kump, L.R., Bai, X., Algeo, T.J., Yang, H., Xie, S., 2011. Nitrogen fixation prevailed simultaneously with the end-Permian marine mass extinction and its implications. Geology 39, 647–650.
Luo, G., Wang, Y., Grice, K., Kershaw, S., Ruan, X., Algeo, T.J., Yang, H., Jia, C., Xie, S., this volume. Microbial-algal community changes during the latest Permian ecological crisis: evidence from lipid biomarkers at Cili, South China. Global and Planetary Change.
Martens, C.S., Klump, J.V., 1984. Biogeochemical cycling in an organic-rich coastal marine basin: 4. An organic carbon budget for sediments dominated by sulfate reduction and methanogenesis. Geochimica et Cosmochimica Acta 48, 1987–2004.
Martin, R.E., 1996. Secular increase in nutrient levels through the Phanerozoic: implications for productivity, biomass, and diversity of the marine biosphere. Palaios 11, 209–219.
Mei, S.L., Henderson, C.M., 2001. Evolution of Permian conodont provincialism and its significance for global correlation and paleoclimate implications. Palaeogeography, Palaeoclimatology, Palaeoecology 170, 237–260.
Meyer, K.M., Kump, L.R., Ridgwell, A., 2008. Biogeochemical controls on photic-zone euxinia during the end-Permian mass extinction. Geology 36, 747–750.
Meyer, K.M., Yu, M., Jost, A.B., Kelley, B.M., Payne, J.L., 2011. $\delta^{13}C$ evidence that high primary productivity delayed recovery from end-Permian mass extinction. Earth and Planetary Science Letters 302, 378–384.
Meyers, P.A., 1997. Organic geochemical proxies of paleoceanographic, paleolimnologic, and paleoclimatic processes. Organic Geochemistry 27, 213–250.
Middelburg, J.J., Soetaert, K., Herman, P.M.J., 1997. Empirical relationships for use in global diagenetic models. Deep-Sea Research I 44, 327–344.
Mizutani, S., 1987. Mesozoic terranes in the Japanese Islands and neighbouring East Asia. In: Scheibner, E. (Ed.), Terrane Accretion and Orogenic Belts: American Geophysical Union Geodynamics Series, 19, pp. 263–273.
Mundil, R., Ludwig, K.R., Metcalfe, I., Renne, P.R., 2004. Age and timing of the Permian mass extinctions: U/Pb dating of closed-system zircons. Science 305, 1760–1763.
Mundil, R., Pálfy, J., Renne, P.R., Brack, P., 2010. The Triassic time scale: new constraints and a review of geochronological data. In: Lucas, S.G. (Ed.), The Triassic Timescale: Geological Society of London Special Publication, 334, pp. 41–60.
Nakrem, H.A., Orchard, M.J., Weitschat, W., Hounslow, M.W., Beatty, T.W., Mork, A., 2008. Triassic conodonts from Svalbard and their boreal correlations. Polar Research 27, 523–539.
Nelson, D.M., Anderson, R.F., Barber, R.T., Brzezinski, M.A., Buesseler, K.O., Chase, Z., Collier, R.W., Dickson, M.-L., Françoise, R., Hiscock, M.R., Honjo, S., Marra, J., Martin, W.R., Sambrotto, R.N., Sayles, F.L., Sigmon, D.E., 2002. Vertical budgets for organic carbon and biogenic silica in the Pacific sector of the Southern Ocean, 1996–1998. Deep-Sea Research II 49, 1645–1674.

Please cite this article as: Algeo, T.J., et al., Plankton and productivity during the Permian–Triassic boundary crisis: An analysis of organic carbon fluxes, Glob. Planet. Change (2012), doi:10.1016/j.gloplacha.2012.02.008

Nie, S., 1991. Paleoclimatic and paleomagnetic constraints on the Paleozoic reconstructions of South China, North China and Tarim. Tectonophysics 196, 279–308.
Nielsen, J.K., Shen, Y., 2004. Evidence for sulfidic deep water during the Late Permian in the East Greenland Basin. Geology 32, 1037–1040.
Ohashi, H., Nakazawa, H., 1996. The microstructure of humic acid–montmorillonite composites. Clay Minerals 31, 347–354.
Ovtcharova, M., Bucher, H., Schaltegger, U., Galfetti, T., Brayard, A., Guex, J., 2006. New Early to Middle Triassic U–Pb ages from South China: calibration with ammonoid biochronozones and implications for the timing of the Triassic biotic recovery. Earth and Planetary Science Letters 243, 463–475.
Patti, B., Guisande, C., Vergara, A.R., Riveiro, I., Maneiro, I., Barreiro, A., Bonanno, A., Buscaino, G., Cuttitta, A., Basilone, G., Mazzola, S., 2008. Factors responsible for the differences in satellite-based chlorophyll *a* concentration between the major global upwelling areas. Estuarine, Coastal and Shelf Science 76, 775–786.
Payne, J.L., Kump, L.R., 2007. Evidence for recurrent Early Triassic massive volcanism from quantitative interpretation of carbon isotope fluctuations. Earth and Planetary Science Letters 256, 264–277.
Payne, J., van de Schootbrugge, B., 2007. Life in Triassic oceans: links between benthic and planktonic recovery and radiation. In: Falkowski, P.G., Knoll, A.H. (Eds.), The Evolution of Primary Producers in the Sea. Academic Press, New York, pp. 165–189.
Payne, J.L., Lehrmann, D.J., Wei, J., Knoll, A., 2006. The pattern and timing of biotic recovery from the end-Permian extinction on the Great Bank of Guizhou, Guizhou Province, China. Palaios 21, 63–85.
Paytan, A., Mackey, K.R.M., Chen, Y., Lima, I.D., Doney, S.C., Mahowald, N., Labiosa, R., Post, A.F., 2009. Toxicity of atmospheric aerosols on marine phytoplankton. Proceedings of the National Academy of Sciences of the United States of America 106, 4601–4605.
Raiswell, R., Berner, R.A., 1987. Organic carbon losses during burial and thermal maturation of normal marine shales. Geology 15, 853–856.
Rampino, M.R., Caldeira, K., 2005. Major perturbation of ocean chemistry and a 'Strangelove Ocean' after the end-Permian mass extinction. Terra Nova 17, 554–559.
Reichow, M.K., Pringle, M.S., Al'Mukhamedov, A.I., Allen, M.B., Andreichev, V.L., Buslov, M.M., Davies, C.E., Fedoseev, G.S., Fitton, J.G., Inger, S., Medvedev, A.Y., Mitchell, C., Puchkov, V.N., Safanova, I.Y., Scott, R.A., Saunders, A.D., 2009. The timing and extent of the eruption of the Siberian Traps large igneous province: implications for the end-Permian environmental crisis. Earth and Planetary Science Letters 277, 9–20.
Retallack, G.J., 1999. Postapocalyptic greenhouse paleoclimate revealed by earliest Triassic paleosols in the Sydney Basin, Australia. Geological Society of America Bulletin 111, 52–70.
Retallack, G.J., 2005. Earliest Triassic claystone breccias and soil-erosion crisis. Journal of Sedimentary Research 75, 679–695.
Retallack, G.J., Jahren, A.H., 2008. Methane release from igneous intrusion of coal during Late Permian extinction events. Journal of Geology 116, 1–20.
Rhodes, M.C., Thayer, C.W., 1991. Mass extinctions: ecological selectivity and primary production. Geology 19, 877–880.
Riccardi, A., Arthur, M.A., Kump, L.R., 2006. Sulfur isotopic evidence for chemocline upward excursions during the end-Permian mass extinction. Geochimica et Cosmochimica Acta 70, 5740–5752.
Rothman, D.H., Forney, D.C., 2007. Physical model for the decay and preservation of marine organic carbon. Science 316, 1325–1328.
Rowan, E.L., Hayba, D.O., Nelson, P.H., Burns, W.M., Houseknecht, D.W., 2003. Sandstone and shale compaction curves derived from sonic and gamma ray logs in offshore wells, North Slope, Alaska—parameters for basin modeling. U.S. Geological Survey, Open-File Report 03–329. http://pubs.usgs.gov/of/2003/of03-329/.
Sansone, F.J., Benitez-Nelson, C.R., Resing, J.A., DeCarlo, E.H., Vink, S.M., Heath, J.A., Huebert, B.J., 2002. Geochemistry of atmospheric aerosols generated from lava–seawater interactions. Geophysical Research Letters 29 (9), 1335. doi:10.1029/2001GL013882, 4 pp.
Schlüter, M., Sauter, E.J., Schäfer, A., Ritzrau, W., 2000. Spatial budget of organic carbon flux to the seafloor of the rate for North Atlantic (60°N–80°N). Global Biogeochemical Cycles 14, 329–340.
Schmoker, J.W., 1977. The relationship between density and gamma-ray intensity in the Devonian shale sequence, Lincoln County, West Virginia. In: Overbey Jr., W.K., Hunt, A.E., Komar, C.A. (Eds.), Proceedings of the First Eastern Gas Shales Symposium. Morgantown Energy Research Center, Morgantown, West Virginia, pp. 266–271.
Schoepfer, S.D., Henderson, C.M., Garrison, G.H., Ward, P.D., 2012. Cessation of a productive coastal upwelling system in the Panthalassic Ocean at the Permian–Triassic boundary. Palaeogeography, Palaeoclimatology, Palaeoecology 313–314, 181–188.
Scotese, C.R., Langford, R.P., 1995. Pangea and the paleogeography of the Permian. In: Scholle, P.A., Peryt, T.M., Ulmer-Scholle, D.S. (Eds.), The Permian of Northern Pangea. : Paleogeography, Paleoclimates, Stratigraphy, 1. Springer-Verlag, Berlin, pp. 3–19.
Sephton, M.A., Looy, C.V., Brinkhuis, H., Wignall, P.B., de Leeuw, J.W., Visscher, H., 2005. Catastrophic soil erosion during the end-Permian biotic crisis. Geology 33, 941–944.
Sheldon, N.D., 2006. Abrupt chemical weathering increase across the Permian–Triassic boundary. Palaeogeography, Palaeoclimatology, Palaeoecology 231, 315–321.
Shen, S.-Z., Henderson, C.M., Bowring, S.A., Cao, C.-Q., Wang, Y., Wang, W., Zhang, H., Zhang, Y.-C., Mu, L., 2010. High-resolution Lopingian (Late Permian) timescale of South China. Geological Journal 45, 122–134.
Shen, S.-Z., Crowley, J.L., Wang, Y., Bowring, S.A., Erwin, D.H., Sadler, P.M., Cao, C.Q., Rothman, D.H., Henderson, C.M., Ramezani, J., Zhang, H., Shen, Y., Wang, X.-D., Wang, W., Mu, L., Li, W.-Z., Tang, Y.-G., Liu, X.-L., Liu, L.-J., Zeng, Y., Jiang, Y.-F., Jin, Y.-G., 2011. Calibrating the end-Permian mass extinction. Science 334, 1367–1372.
Shen, J., Algeo, T.J., Zhou, L., Feng, Q., Yu, J., Ellwood, B.B., 2012. Volcanic perturbations of the marine environment in South China preceding the latest Permian extinction event and their biotic effects. Geobiology 10, 82–103.
Song, H.Y., Tong, J.N., Algeo, T.J., Qiu, H.O., Song, H.J., Tian, L., Chen, Z.Q., this volume. Large shallow-to-deep $\delta^{13}C$ gradients in Early Triassic seas of the South China craton. Global and Planetary Change.
Stampfli, G.M., Borel, G.D., 2001. A plate tectonic model for the Paleozoic and Mesozoic constrained by dynamic plate boundaries and restored synthetic oceanic isochrones. Earth and Planetary Science Letters 196, 17–33.
Sugiyama, K., 1997. Triassic and Lower Jurassic radiolarian biostratigraphy in the siliceous claystone and bedded chert units of the southeastern Mino Terrane, Central Japan. Bulletin of the Mizunami Fossil Museum 24, 79–193.
Thompson, E., 2000. Paleocene chemical paleoceanography; global paleoproductivity and regional (North Sea) paleoclimate. Ph.D. dissertation, Goteborg University, Goteborg, Sweden.
Tong, J., Zhang, S., Zuo, J., Xiong, X., 2007. Events during Early Triassic recovery from the end-Permian extinction. Global and Planetary Change 55, 66–80.
Tribovillard, N., Riboulleau, A., Lyons, T., Baudin, F., 2004. Enhanced trapping of molybdenum by sulfurized organic matter of marine origin as recorded by various Mesozoic formations. Chemical Geology 213, 385–401.
Tyson, R.V., 2001. Sedimentation rate, dilution, preservation, and total organic carbon: some results of a modelling study. Organic Geochemistry 32, 333–339.
Tyson, R.V., 2005. The "productivity versus preservation" controversy; cause, flaws, and resolution. In: Harris, N.B. (Ed.), Deposition of Organic-Carbon-Rich Sediments: Models Mechanisms, and Consequences: Society for Sedimentary Geology (SEPM-SSG) Special Publication, 82, pp. 17–33.
Vetö, I., Demeny, A., Hertelendi, E., Hetenyi, M., 1997. Estimation of primary productivity in the Toarcian Tethys: a novel approach based on TOC, reduced sulphur and manganese contents. Palaeogeography, Palaeoclimatology, Palaeoecology 132, 355–371.
Wang, C., Visscher, H., 2007. Abundance anomalies of aromatic biomarkers in the Permian–Triassic boundary section at Meishan, China—evidence of end-Permian terrestrial ecosystem collapse. Palaeogeography, Palaeoclimatology, Palaeoecology 252, 291–303.
Ward, P.D., Montgomery, D.R., Smith, R., 2000. Altered river morphology in South Africa related to the Permian–Triassic extinction. Science 289, 1730–1743.
Wiesner, M.G., Wang, Y., Zheng, L., 1995. Fallout of volcanic ash to the deep South China Sea induced by the 1991 eruption of Mount Pinatubo (Philippines). Geology 23, 885–888.
Wignall, P.B., 2007. The End-Permian mass extinction—how bad did it get? Geobiology 5, 303–309.
Winguth, A.M.E., Maier-Reimer, E., 2005. Causes of marine productivity and oxygen changes associated with the Permian–Triassic boundary: a reevaluation with ocean general circulation models. Marine Geology 217, 283–304.
Winguth, C., Winguth, A.M.E., 2012. Simulating Permian–Triassic oceanic anoxia distribution: implications for species extinction and recovery. Geology 40, 127–130.
Wright, J., Colling, A., 1995. Seawater: Its Composition, Properties and Behaviour, 2nd Ed. Pergamon, Oxford. (168 pp.).
Xia, W., Zhang, N., Kakuwa, Y., Zhang, L., 2005. Radiolarian and conodont biozonation in the pelagic Guadalupian–Lopingian boundary interval at Dachongling, Guangxi, South China, and mid-upper Permian global correlation. Stratigraphy 2, 217–238.
Xie, S., Pancost, R.D., Yin, H., Wang, H., Evershed, R.P., 2005. Two episodes of microbial change coupled with Permo/Triassic faunal mass extinction. Nature 434, 494–497.
Xie, S., Pancost, R.D., Huang, X., Jiao, D., Lu, L., Huang, J., Yang, F., Evershed, R.P., 2007. Molecular and isotopic evidence for episodic environmental change across the Permo/Triassic boundary at Meishan in South China. Global and Planetary Change 55, 56–65.
Xie, S., Pancost, R.D., Wang, Y., Yang, H., Wignall, P.B., Luo, G., Jia, C., Chen, L., 2010. Cyanobacterial blooms tied to volcanism during the 5 m.y. Permo-Triassic biotic crisis. Geology 38, 447–450.
Xu, L., Lin, Y., Shen, W., Qi, L., Xie, L., Ouyang, Z., 2007. Platinum-group elements of the Meishan Permian–Triassic boundary section: evidence for flood basaltic volcanism. Chemical Geology 246, 55–64.
Yin, H., Huang, S., Zhang, K., Hansen, H.J., 1992. The effects of volcanism on the Permo-Triassic mass extinction in South China. In: Sweet, W.C., Yang, Z.Y., Dickins, J.M., Yin, H.F. (Eds.), Permo-Triassic Events in the Eastern Tethys. Cambridge University Press, Cambridge, pp. 146–157.
Yin, H.F., Zhang, K.X., Tong, J.N., Yang, Z.Y., Wu, S.B., 2001. The Global Stratotype Section and Point (GSSP) of the Permian–Triassic boundary. Episodes 24, 102–114.
Zaback, D.A., Hayes, J.M., Pratt, L.M., 1993. Transport and reduction of sulfate and immobilization of sulfide in marine black shales. Geology 21, 141–144.
Zhao, L., Orchard, M.J., Tong, J., Sun, Z., Zuo, J., Zhang, S., Yun, A., 2007. Lower Triassic conodont sequence in Chaohu, Anhui Province, China and its global correlation. Palaeogeography, Palaeoclimatology, Palaeoecology 252, 24–38.

Please cite this article as: Algeo, T.J., et al., Plankton and productivity during the Permian–Triassic boundary crisis: An analysis of organic carbon fluxes, Glob. Planet. Change (2012), doi:10.1016/j.gloplacha.2012.02.008